J. Fluid Mech. (2009), *vol.* 629, *pp.* 343–374.
doi:10.1017/S0022112009006405 Printed in the United Kingdom

PIV measurements of flow through a model porous medium with varying boundary conditions

JAMES K. ARTHUR,
DOUGLAS W. RUTH† AND MARK F. TACHIE

Department of Mechanical and Manufacturing Engineering, University of Manitoba, Winnipeg, Manitoba R3T 5V6, Canada

(Received 9 July 2008 and in revised form 30 January 2009)

This paper reports an experimental investigation of pressure-driven flow through models of porous media. Each model porous medium is a square array of circular acrylic rods oriented across the flow in a rectangular channel. The solid volume fraction ϕ of the arrays ranged from 0.01 to 0.49. Three boundary conditions were studied. In the first boundary condition, the model porous medium was installed on the lower wall of the channel only and was bounded by a free zone. In the second and third boundary conditions, porous media of equal and unequal ϕ were arranged on the lower and upper channel walls so that the two media touched (second boundary condition), and did not touch (third boundary condition). Using water as the working fluid, the Reynolds number was kept low so that inertia was not a factor. Particle image velocimetry was used to obtain detailed velocity measurements in the streamwise-transverse plane of the test section. The velocity data were used to study the effects of ϕ and the different boundary conditions on the flow through and over the porous medium, and at the interface. For the first boundary condition, it was observed that at $\phi = 0.22$, flow inside the porous medium was essentially zero, and the slip velocity at the porous medium and free zone interface decayed with permeability. In the second and third boundary conditions, flow communication between the porous media was observed to be dependent on the combinations of ϕ used, and the trends of the slip velocities at the interface between the two porous media obtained for that boundary condition were indicative of complicated interfacial flow.

1. Introduction

The study of flow through porous media is fundamental to many engineering fields. Some important applications are oil and gas reservoirs, groundwater hydrology, filters, polymer brushes and heat pipe technology. Due to its practical and fundamental importance, the study of flow phenomena through porous media has attracted considerable research interest. Publications by Bear (1972), Scheidegger (1974), Greenkorn (1983), Nield & Bejan (1992) and Huang & Ayoub (2008) provide reviews of related research developments in the literature.

While some porous media flows may be driven by shear as in the case of a polymer brush, in many other applications, such as oil and gas exploration, the flows are generated by a pressure gradient. Many industrial processes such as the recovery of

† Email address for correspondence: druth@cc.umanitoba.ca

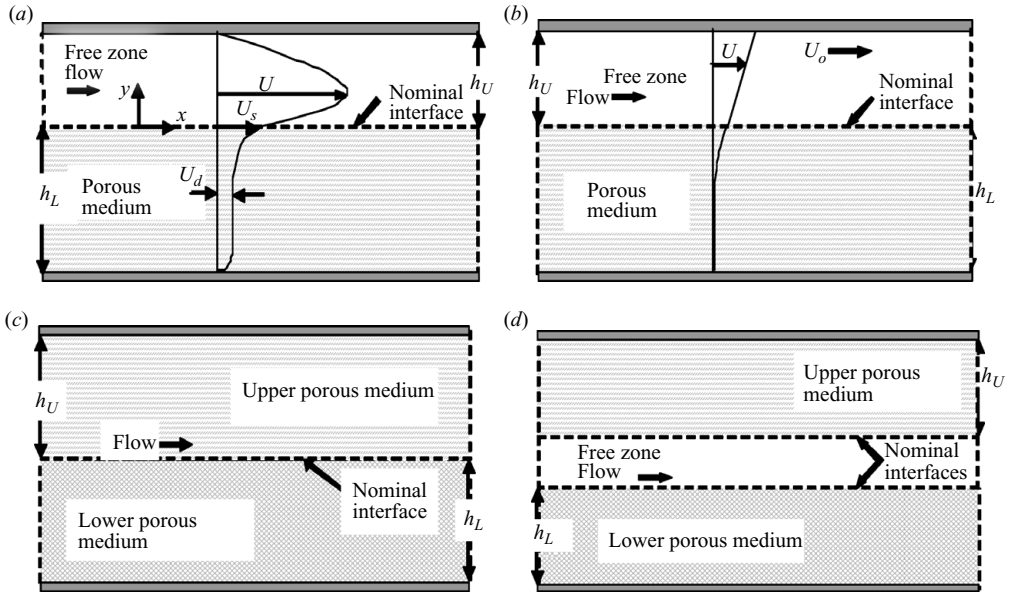

FIGURE 1. Flow through a porous medium in (*a*) and (*b*) bounded by a free zone; the velocity (U) profiles for a given streamwise location in the flow for a (*a*) pressure-driven, and (*b*) shear-driven case; (*c*) bounded by another porous medium, with the media touching; and (*d*) bounded by another porous medium, but with a free zone between the porous media. The dimensions h_L and h_U represent different depths.

oil and the manufacturing of advanced composites are typically done by injecting some fluid by means of pressure. Even in a polymer brush on suspended particles, pressure gradient may be a factor if the polymer chains are attached to a stationary surface (Tachie, James & Currie 2004). Although flows through porous media may be multi-phase, and may show the presence of inertial effects, the scope of the present study is limited to that of single-phase flows, and those for which inertia is not a factor. However, this study still provides basic information that relates to the more complex, above-mentioned practical examples.

As schematized in figures 1(*a*, *b*) and 1(*c*, *d*), respectively, flow through a porous medium may be bounded by a region of simple fluid flow, (i.e. a free zone), or by another porous medium. In the latter condition, the lower and upper media may be touching as illustrated in figure 1(*c*). This is what prevails in media filters, and aquifers and oil reservoirs composed of adjoining layers of varying solid volume fraction. In other applications such as fluid flow through fractured rocks and filtration cross-flow problems, the lower and upper porous surfaces of equal or different solid volume fractions are separated by a free zone. This is the condition shown in figure 1(*d*). In all the boundary conditions described above, the porous media are bounded on one side by an impermeable wall. As mentioned earlier, the flow may be driven by shear or a pressure gradient, and typical velocity distributions for pressure- and shear-driven flows are shown in figures 1(*a*) and 1(*b*), respectively. (In figure 1*b*, U_o is the velocity of the upper wall.)

Studies of flow through porous media have been conducted using a variety of models of porous media to represent the real porous media (as reviewed by Larson & Higdon 1986). The present study focuses on flow through and over model porous media made up of square arrays of cylinders, and seeks to build upon the foundation

of previous studies done using this kind of model. The value of such a model lies in its simplicity for adaptation in theoretical, numerical and experimental studies. These studies can in turn be used to simulate real cases such as mammalian hair, leather, polymer chains and banks of heat exchanger tubes. They may even provide useful understanding about the dynamics of flow through oil, gas and water reservoirs.

1.1. *Flow through a porous medium, bounded by a free zone*

Flow through a porous medium bounded by a free zone (i.e. figures 1*a* and 1*b*) has been studied extensively using various analytical, numerical and experimental techniques. Some of the relevant studies are reviewed in this section.

For the case indicated in figure 1(*a*), a pressure-driven flow may be specified so that the region $y < 0$ is occupied by a model porous medium of a regular array of rods, saturated with a fluid identical to that in $y > 0$. The flow inside the porous medium, if sufficiently slow, is governed by Darcy's law, equivalently stated (Gupte & Advani 1997) as

$$\nabla p = -\frac{\mu \cdot U}{k}, \tag{1.1}$$

where ∇p is the applied pressure gradient, μ is the fluid dynamic viscosity and U is the superficial velocity (volumetric flow rate per unit area). The quantity k is the specific Darcy permeability, obtained by empirical means. For a homogeneous model porous medium made up of a square array of long circular cylinders with uniform diameter, k is given by (Sangani & Acrivos 1982; Jackson & James 1986)

$$\frac{k}{r^2} = \frac{1}{8\phi}[-\ln\phi - 1.476 + 2\phi - 1.774\phi^2 + 4.076\phi^3], \tag{1.2}$$

where r and ϕ are, respectively, the radius of the cylinder cross-section and the solid volume fraction. The laminar flow in the free zone may be modelled by the Navier–Stokes equation. With appropriate modifications in the case of a steady slow flow, this equation is given by

$$\nabla^2 u = \nabla p. \tag{1.3}$$

To establish a continuity of fluid velocities and stresses to match the Darcian regime and the Navier–Stokes free zone, the following modification of Darcy's law by Brinkman (1947) is frequently used:

$$\frac{\mu \cdot U}{k} = -\nabla p + \mu' \nabla^2 U \tag{1.4}$$

where μ' is an apparent (Brinkman) viscosity. The literature has been mixed about the value of μ'. This viscosity may be dependent on the geometry and structure of the porous medium as well as the flow conditions. Brinkman (1947), for example, calculated the viscous force exerted by a flowing fluid on a dense swarm of particles based on a model of a spherical particle embedded in a porous mass, and recommended that $\mu = \mu'$ (i.e. the Brinkman model). Larson & Higdon (1986, 1987) also studied the shear flow near the surface of a model porous medium made up of square and hexagonal arrays of cylindrical inclusions. They found that $\mu < \mu'$ when the flow was parallel to the cylinders, and $\mu > \mu'$ when the flow was perpendicular to the cylinders. In one notable derivation of (1.4), Ochoa-Tapia & Whitaker (1995) have shown that $\mu'/\mu = 1/(1-\phi)$. They pointed out that the concept of Brinkman viscosity is a confusion of a superficial and an intrinsic property.

Nonetheless, apart from the use of (1.4), the problem of flow through porous medium bounded by a free zone can be solved by specifying appropriate hydrodynamic

boundary conditions at the nominal interface between the porous medium and the free zone. The reader may refer to the literature (e.g. Ochoa-Tapia & Whitaker 1998; Alazmi & Vafai 2001; Breugem, Boersma & Uittenbogaard 2005; Deng & Martinez 2005; Chandesris & Jamet 2006; Rosenzweig & Shavit 2007) for a more detailed discussion of various boundary conditions. Some of these conditions have been obtained upon the assumption of a slip velocity U_s at the nominal interface. The slip velocity is known to be significant in cases where $\phi < 0.10$, as in non-inertial flows over fibrous porous media (James & Davis 2001; Davis & James 2003). One of the foremost empirical interfacial boundary conditions proposed in the literature that features U_s is that of Beavers & Joseph (1967). In the case of figure 1(a), that boundary condition can be expressed as

$$\left.\frac{\mathrm{d}U}{\mathrm{d}y}\right|_{y=0+} = \frac{\alpha}{\sqrt{k}}(U_s - U_d), \tag{1.5}$$

where $\mathrm{d}U/\mathrm{d}y|_{y=0+}$ is the shear rate of the fluid at the interface, α is the slip coefficient and $U_d = -\nabla pk/\mu$ is the superficial velocity in the porous medium. There have been many studies to investigate (1.5) experimentally (e.g. Beavers, Sparrow & Magnuson 1970; Taylor 1971; Gupte & Advani 1997), theoretically (e.g. Richardson 1971; Saffman 1971) and numerically (e.g. Sahraoui & Kaviany 1992). It has been observed that α is dependent on certain factors such as interface location, surface micro-structure, ϕ, Reynolds number based on the Darcy velocity, channel depth and the bulk flow direction (Beavers *et al.* 1970; Saffman 1971; Sahraoui & Kaviany 1992; James & Davis 2001).

If the depth of the porous medium in figure 1(a) is large, such that the lower solid wall effects are insignificant (as in an 'unbounded' porous media), (1.4) and (1.5) can be shown to be related. Because $U \to U_d$ as $y \to -\infty$, and $U = U_s$ at $y = 0$, the solution of a one-dimensional Poiseuille flow in (1.4), valid in the region $y \leqslant 0$ is (Gupte & Advani 1997)

$$U = U_d + (U_s - U_d)\exp\left[\frac{y}{\sqrt{[k\,(\mu'/\mu)]}}\right]. \tag{1.6}$$

Differentiating (1.6) once with respect to y, and evaluating at $y = 0$ yields

$$\left.\frac{\mathrm{d}U}{\mathrm{d}y}\right|_{y=0} = \frac{1}{\sqrt{[k(\mu'/\mu)]}}(U_s - U_d). \tag{1.7}$$

This equation demonstrates the equivalence of (1.4) and (1.5) when $\alpha = \sqrt{(\mu/\mu')}$.

For studies of flows through and over a porous medium of a square array of cylinders, U_s has been used to learn more about the penetration of the free zone flow into the porous medium. In one such study, James & Davis (2001) used singularity methods to solve flows driven by shear and pressure in the interfacial region between a porous medium and a free zone. The authors introduced a dimensionless slip velocity $U_s/(\dot{\gamma}\sqrt{k})$ (where $\dot{\gamma} = \mathrm{d}U/\mathrm{d}y|_{y=0+}$) that allowed for the assessment of flow penetration relative to the local conditions of flow. It should be noted that $U_s/(\dot{\gamma}\sqrt{k}) = 1/\alpha$ in (1.5) if the value of U_d is negligibly small. In the present study, values of α reported in the literature will henceforth be expressed in terms of $U_s/(\dot{\gamma}\sqrt{k})$ because U_s is a quantity of prime interest. James & Davis (2001) found that for a shear-driven flow, $U_s/(\dot{\gamma}\sqrt{k})$ depends weakly on ϕ. For pressure-driven flow, U_s was also found to be less than that for comparable shear flow. The depth of penetration of flow in the free zone into the porous medium was also only a fraction of what can be deduced from the

Brinkman's model. They thus demonstrated that (1.4) cannot be applied to the flow cases they studied. In a later analytical work, Davis & James (2003) used singularity methods to investigate the slip velocity at the interface of a regular array of rods and the unfilled portion of the annulus for a shear-driven flow. Solid volume fractions ranging from 0.0001 to 0.10 were studied. The dimensionless velocity, $U_s/(\dot{\gamma}\sqrt{k})$ was found to be nearly independent of the number of annular rows behind the rods.

Tachie, James & Currie (2003) performed experiments to validate the Couette flow studies of James & Davis (2001) and Davis & James (2003). The porous media used were of circular, square and equilateral triangular cross-sections. It was also found that $U_s/(\dot{\gamma}\sqrt{k})$ decayed from 0.30 to 0.24 as ϕ increased from 0.01 to 0.16. The dimensionless interfacial slip velocity $U_s/(\dot{\gamma}\sqrt{k})$ was also confirmed to be nearly independent of the rod shape, and the number of circles of rods forming an array. Davis & James (2004) analysed the simple shear flow field over square arrays of model porous media. The porous media was composed of circular rods of ϕ ranging from 0.001 to 0.100, aligned in the direction of flow, and occupying a fraction of the channel. They noted that the $U_s/(\dot{\gamma}\sqrt{k})$ was independent of the number of rows and of the fraction of the channel depth filled by the porous medium (filling fraction). Concurring with Larson & Higdon (1986, 1987), their results affirmed that penetration in 'aligned flow' was greater than that in 'cross-flow'. Furthermore, they pointed out that the Brinkman model could not provide a reasonable estimate for the velocity at the edge of their model porous medium. Tachie *et al.* (2004) subsequently investigated slow flow through a model brush. The test facility and experimental technique employed were similar to that used in Tachie *et al.* (2003). Here, however, the model porous media used consisted of an array of uniformly spaced rods oriented perpendicular to simulate a three-dimensional 'brush-flow' configuration of 0.81 filling fraction. PIV was used to study the velocity field in the penetration region of brushes of solid volume fractions 0.025, 0.05 and 0.10. The dimensionless slip velocity, $U_s/(\dot{\gamma}\sqrt{k})$, was found to be about 1, and nearly independent of ϕ. It was noted that the 'brush-flow' configuration gave higher slip velocities, and greater penetration in flow compared with the 'cross-flow' case.

More recently, Agelinchaab, Tachie & Ruth (2006) used the PIV technique to study the velocity field in a pressure-driven flow through a model three-dimensional porous media bounded by a free zone. The model porous media were made up of cylindrical rods in a square array of $0.01 \leqslant \phi \leqslant 0.49$. For a constant channel depth H, their results revealed that the velocity within the porous medium increased with both rod spacing l and rod height h but decreased with ϕ. In the free zone, however, the velocity increased with h and ϕ, but decreased with increasing l. The dimensionless slip velocity, $U_s/(\dot{\gamma}\sqrt{k})$ for h/H (filling fraction) $= 0.28$ and 0.56 were about 1 and 2, respectively.

From this summary, it is clear that amongst the boundary flow conditions shown in figure 1, there have been many experimental, theoretical and numerical studies focused on the flow bounded by a free zone. Much insight has been gained about the applicability of (1.4) and (1.5) in various arrangements of porous media made up of a regular array of cylindrical rods, and driven by shear or pressure. Very useful evaluations have been made to assess the levels of penetration of the free zone flow into the porous medium. However, these studies have been mostly limited to the interfacial region. Thus, very little information exists in the literature (perhaps, apart from Agelinchaab *et al.* 2006) that gives detailed velocity measurements of flow through and over model porous medium for a wide range of ϕ. Such data is needed for the validation of future numerical simulations of porous media flows bounded

by a free zone. Furthermore, the literature falls short of providing much information about the relative distributions of flow expected to be channelled into the free zone, or into the porous medium.

1.2. *Flow through a porous medium, bounded by another porous medium*

The literature reports very few studies of flow through two bounding porous media (figure 1*c*). The studies that are reported are theoretical calculations, and for cases where one or more of the porous media are affected by inertia. Vafai & Thyagaraja (1987) analysed the velocity fields and heat transfer for three kinds of interfacial zones. They are (i) the interface between two different porous media, (ii) the interface between a porous medium and a free zone and (iii) the interface between a porous medium and an impermeable medium. Their solutions pertained to pressure-driven flow fields, and the porous media were assumed to be unbounded at one end. The velocity fields were also specified to be independent of the flow direction, and inertial effects were considered. For the case of the flow through a porous medium bounded by another porous medium, analytical solutions for the interfacial flow were obtained by employing continuity of velocities and stresses at the interface. The interface velocity was solved in terms of ratios of material properties and parameters such as the permeability, porosity and pressure gradient. The analytical solutions were compared with numerical results obtained by finite differencing the governing equations, and agreements between the two were reasonable. By keeping the permeability of the upper porous medium constant, they found out that the velocity at the interface tended asymptotically towards zero when the permeability and porosity of the lower porous medium tended towards zero. Although the results of this work concur with predictions based on physical principles, the cases analysed were only those of simplified unidirectional flows. The analytical study could therefore not provide the details of complex interactions (communication) between adjoining layers of porous media associated with a three-dimensional flow.

Allan & Hamdan (2002) also investigated the interfacial flow between two porous layers of different structures. In one of the layers, the flow was assumed to be governed by the Forchheimer equation while the other was assumed to be governed by the Brinkman equation. The velocities and shear stresses at the interface between the layers were matched in this work. Although the work indicates the influence of Reynolds number and Darcy number on the flow through the porous media, it provides no further details about the relative flow distributions that should be expected in either medium.

In summary, the literature provides no detailed experimental investigation of fluid flow through and over a porous medium bounded by another porous medium. As a result, many important questions about flow distribution between layers of porous media of the same solid volume fraction or of different solid volume fractions remain unresolved. Questions about penetration of flow through layers of porous media with an intermediate free zone (as shown in figure 1*d*) are also not well understood because there is no experimental data in the literature of such an arrangement known to the authors. The study of porous medium flow bounded by another porous medium is needed to provide information to model and improve design of engineering systems such as media filters, and may give some insight to the flow dynamics through fractures in porous rocks.

1.3. *Objectives and scope*

From the foregoing discussion, it is clear that of the boundary flow conditions shown in figure 1, there has been much more experimental, theoretical and numerical work

focused on the flow through a porous medium bounded by a free zone. Even in those studies however, there has been little or no attempt to quantify the flow distributions into the free zone, or the porous medium for a wide range of ϕ. For flow through two adjoining porous media, there is no experimental data showing the details of flow communication between the media. Furthermore, there are few experimental treatments given in the literature for single-phase flows through two porous media, separated by a free zone.

The main goal of this research therefore, is to study the effects of varying the boundary conditions on a flow through a porous medium (as shown in figure 1). For flow through a porous medium bounded by a free zone, the study aims at studying the effects of ϕ, quantifying the percentage distributions through the free zone and porous medium and studying the flow at the nominal interface between the free zone and the porous medium. For flow through a porous medium bounded by another porous medium, where the porous media are respectively touching and not touching (i.e. separated by a free zone), the objectives are to provide insight about the modes of communication between the porous media, and to provide information about the flow at the various interfaces. These objectives are met by analysing velocity data obtained from PIV measurements made in a pressure-driven flow through and over model three-dimensional porous media covering a wide range of solid volume fraction ($0.01 \leqslant \phi \leqslant 0.49$).

It should be noted that several experimental studies of transport through porous media have been conducted in the past using various non-intrusive measurement techniques (e.g. Stephenson & Stewart 1986; Yarlagadda & Yoganathan 1989; Saleh, Thovert & Adler 1992; Peurrung, Rashidi & Kulp 1995; Gupte & Advani 1997; Khalili *et al.* 1999; Moroni & Cushman 2001; Ogawa *et al.* 2001; Moroni, Kleinfelter & Cushman 2007; Huang *et al.* 2008). As a non-intrusive technique for velocity measurement, PIV has been widely used to make pore-scale two-dimensional velocity component (e.g. Northrup *et al.* 1993) and three-dimensional velocity component (e.g. Rashidi *et al.* 1996; Rosenzweig & Shavit 2007) measurements of flow through various porous media. PIV has also been used in various experimental studies using porous medium of an array of cylindrical rods. Such studies include that of Shams, James & Currie (2003) and Tachie *et al.* (2003), who made two-dimensional velocity component measurements of shear-driven flow bounding a porous medium. Tachie *et al.* (2004) and Agelinchaab *et al.* (2006) also measured the three-dimensional velocity components of flow through and over porous media of different configurations, and driven by shear and pressure, respectively. The PIV technique makes it possible for large portions of flow fields to be measured instantaneously (Raffel *et al.* 2007). The present study however provides only two-dimensional whole-field velocity components measurements in two planes (where changes of velocity distributions are most dramatic) for the various porous media configurations.

The porous media models used in this study consist of transparent acrylic circular rods arranged in a square array, and installed across the flow, in a rectangular channel. The models were initially installed on the lower wall of the channel only, to simulate flow through a porous medium bounded by a free zone (as shown in figure 1*a*). This is similar to the set-up of Agelinchaab *et al.* (2006). However, the present study expands the scope of previous studies by testing for the cases where the flow through the porous medium is bounded by another porous medium. This is accomplished by installing model porous media of equal or unequal ϕ on both lower and upper walls of the channel. The depth of the channel was varied to provide conditions for which the lower and upper porous media touched (as in figure 1*c*), and did not touch each

other (as in figure 1*d*). In the present experiments, the Reynolds number was kept low so that inertia effects were negligible. Averaging of velocity distributions between adjacent rod centres was also performed for the planes of measurement. From the results obtained, the effects of ϕ and different boundary conditions on the velocity distribution, as well as the modes of communication between layers of porous media were studied. Consequently, the fluid flow in the respective interfacial zones was examined.

2. Experimental apparatus and measurement procedure

2.1. *Test facility*

The experiments were performed in a rectangular channel. Schematic diagrams of the channel and arrangements of the test models are shown in figure 2. To facilitate optical access, the test section and porous media models were constructed from transparent acrylic material, of refractive index 1.47. The test channel was of length $L = 600$ mm, width $W = 71$ mm and of a variable depth H. The channel depth could be varied by placing machined transparent acrylic plates of specific thicknesses on the lower wall. The porous media models were constructed by inserting circular rods into holes drilled into the plates. The rods were arranged in square arrays to obtain solid volume fractions in the desired range of $0.01 \leqslant \phi \leqslant 0.49$. For a given rod diameter d and a given ϕ, the spacing between rods l was determined from the relation

$$l = d/2\sqrt{(\pi/\phi)} \tag{2.1}$$

Three different rod diameters – that is, $d = 1.59$, 3.18 and 4.76 mm – and three different spacing between adjacent rods – that is, $l = 6.03$, 8.90 and 12.60 mm – were used to achieve the range of ϕ stated above. In order to ensure that the flow inside the model porous medium developed to become periodic (as will be shown later), each porous medium had between 6 and 10 rows of rods along the direction of flow and spanned the entire width of the channel. Porous media rods of mean heights, $h_L = 14$ mm and $h_U = 7$ mm were used for the lower and upper channel walls, respectively, to test specific boundary conditions. The relative standard deviation of the lower and upper porous media rod heights from the mean were about 2.5 % and 1.5 %, respectively. The centre of the most upstream columns of rods was located 400 mm downstream from the inlet of the test section. This was done to ensure that laminar flow in the empty channel (that is, a channel with no porous media present) would be fully developed at that location.

In figure 2, the coordinate system used in this work is also shown. The streamwise, transverse and spanwise directions are, respectively, denoted by x, Y(or y) and z. The location $x = 0$ coincides with the centre of the most upstream columns of rods. For the transverse direction, the following references are used: $Y = 0$ is the centreline between the lower and upper walls; $y_1 = 0$ is at the interface between the lower porous medium and a free zone (as in boundary condition of figure 2*b*); $y_2 = 0$ is also the interface between the upper porous medium and a free zone (as in boundary condition of figure 2*d*). For the spanwise direction, $z = 0$ is fixed at the channel mid-span.

A centrifugal pump supplied by the Cole-Parmer Instruments Company and of maximum flow rate 530.4 $\mathrm{cm^3\ s^{-1}}$ was used to deliver a non-pulsating low-pressure flow into the channel. Water of kinematic viscosity $\nu = 1.0 \times 10^{-6}\ \mathrm{m^2\ s^{-1}}$ at 20°C, density $\rho = 998\ \mathrm{kg\ m^{-3}}$ and a refractive index 1.33 was used as the working fluid.

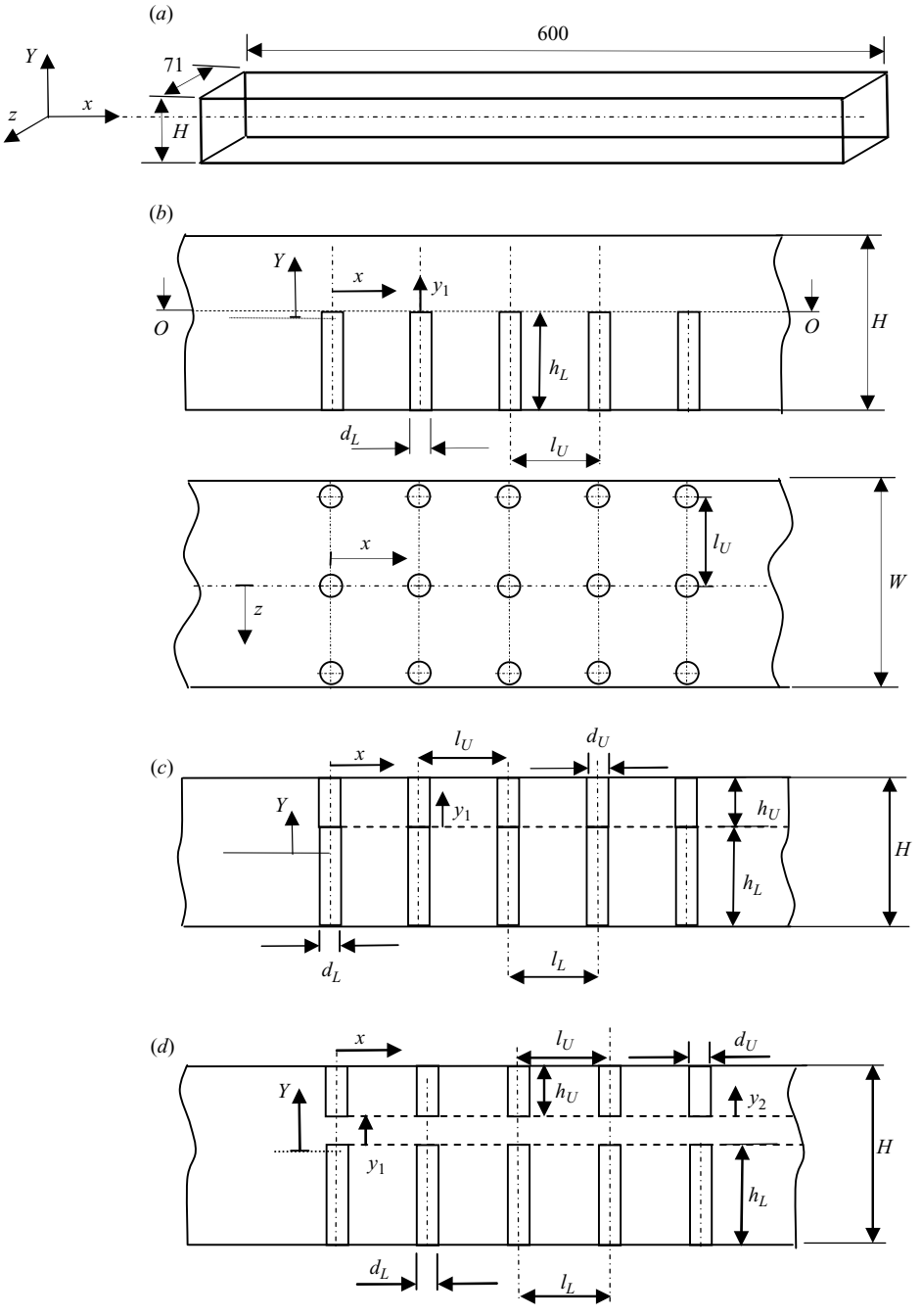

FIGURE 2. Schematic drawings of (*a*) the test section; (*b*) sectioned (O–O) front and top views showing arrangements of model porous medium on lower wall of the channel only; front views of (*c*) lower and upper walls of the channel, with the media touching; (*d*) lower and upper walls of the channel, with the media not touching. The coordinate system used in this work is also shown. All interfaces are represented by dashed lines. All numeric dimensions are in millimetres.

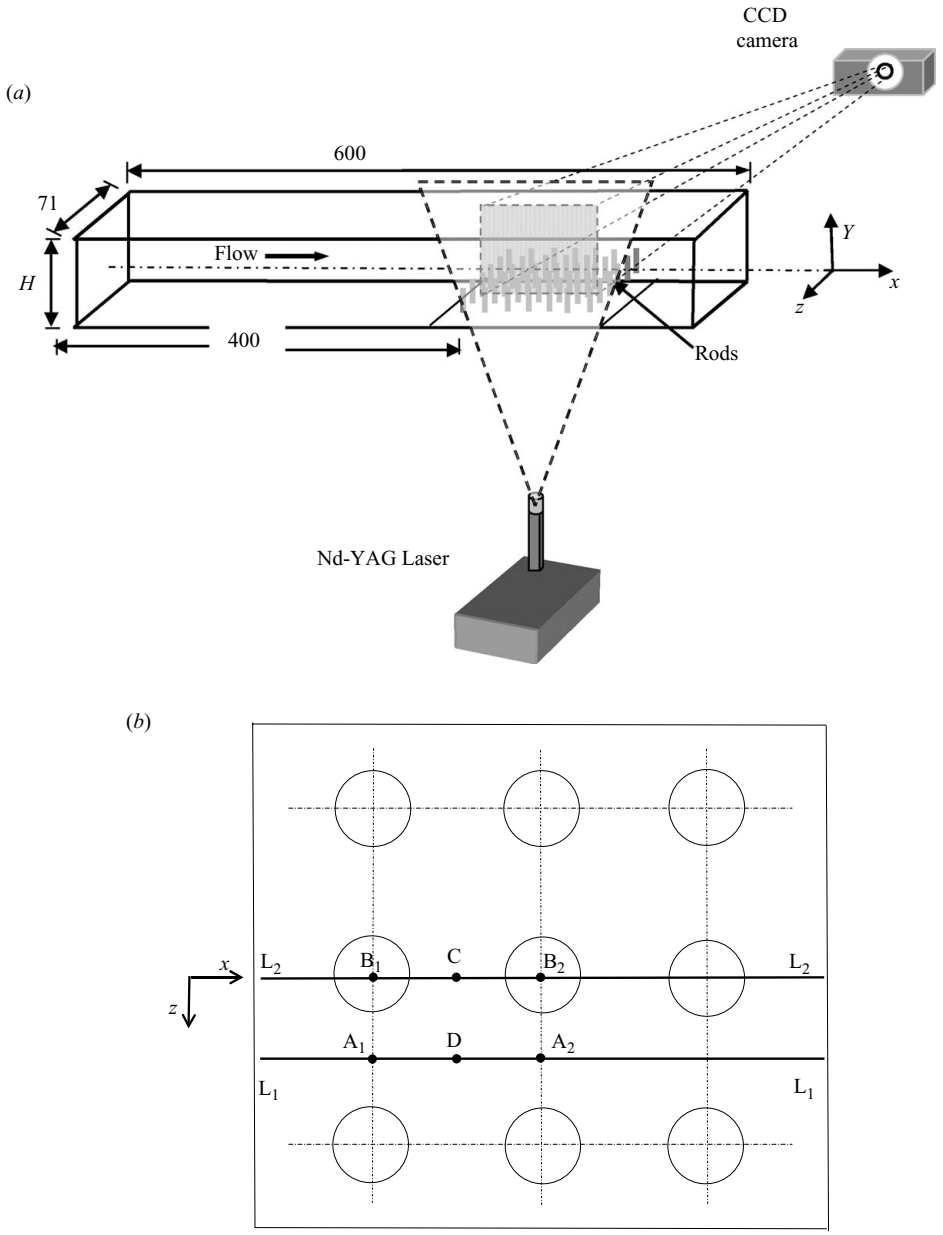

FIGURE 3. Schematic drawings of (*a*) the channel and PIV set-up; and (*b*) top view of a model porous medium with the laser sheet of light represented by line segments: L_1-L_1. and L_2-L_2. Other representative reference locations are also shown. All numeric dimensions are in millimetres.

2.2. *The PIV system and velocity measurements*

A schematic illustration of the PIV and channel arrangement is shown in figure 3(*a*). The flow was seeded using fluorescent polymer micro-sphere particles supplied by Duke Scientific Corporation with mean diameter and specific gravity, of 6 μm and 1.05, respectively. An Nd-YAG 120 mJ per pulse laser and 532 nm wavelength was

used to illuminate the flow field. A set of cylindrical lens was used to convert the laser light into a thin sheet. The laser sheet was positioned in a plane perpendicular to the camera. The seeding particles absorb and emit light at wavelengths of 542 and 612 nm, respectively, helping to filter distortion effects. The particle settling velocity and response time were estimated to be $1.34\,\mu\text{m s}^{-1}$ and 37.4 ps, respectively. Because these two values are very small compared with typical velocity and time scales used in the experiment, the particles were considered to follow the fluid faithfully.

A C–mount 58–62 mm diameter EX Sigma lens, equipped with a band-pass filter was fitted to a Dantec Dynamic HiSense 4M digital camera using a charged-couple devise (CCD). The CCD camera, of 2048 pixel $\times$ 2048 pixel chip and pitch $7.4\,\mu$m, was used to capture images of the flow field. To minimize errors due to peak locking while optimizing background contrast and resolution, a focal length of 11 and field of view of 46.5 mm $\times$ 46.5 mm were used in the measurement process. The particle image diameter was estimated to be 2.57 pixels. This value is close to the recommended optimum value of 2 pixels required to minimize peak locking (Raffel *et al.* 2007). During the image acquisition, the time between the pulses of the laser was chosen so that the maximum particle displacement in an interrogation area (IA) was less than a quarter of the side of the IA (Prasad, 2000). The images were stored continuously through a buffer system onto a desktop computer. The digital images were post-processed using the adaptive-correlation option of Flow Manager 4.50.17, a commercial software developed by Dantec Dynamics. The adaptive correlation uses a multi-pass Fast Fourier Transform cross-correlation algorithm to determine the average particle displacement within the IA during a period of laser exposures. A Gaussian window function of width 0.1 pixels was used as the input filter to the correlation algorithm. A low-pass Gaussian output filter of width 1.8 pixels was applied on the correlation plane before peak detection. Two steps of adaptive correlation processing were used. To allow for a good number of valid vectors, the initial IA was set to a size of 64 pixels $\times$ 64 pixels. Two iterations were performed at the first step of the processing, followed by another at the final step. Thus, each image was subdivided into 32 pixels $\times$ 32 pixels and processed with 50 % $\times$ 50 % overlap to give a spatial resolution of 0.36 mm $\times$ 0.36 mm IA. Further smoothing of the resultant vectors was done by using a moving average validation option over a neighbourhood size of 3 pixels $\times$ 3 pixels. Three iterations were done in the validation process, using an acceptance factor of 0.05.

In anticipation of a three-dimensional flow in the porous medium, measurements needed to be taken at several locations along the entire channel span. It would have been ideal to take velocity measurements at several horizontal cross-sections to completely characterize the three-dimensional flow, as in Agelinchaab *et al.* (2006) (where there were model porous media on the lower channel wall only). However, this was not possible due to the reduced optical access associated with the case of porous media models installed on both channel walls, as used in the present study. Furthermore, preliminary experimental results (using a similar set-up and test conditions) of streamlines for the horizontal plane, showed that major changes were apparent when the patterns at the locations between adjacent rod centres and at the rods were compared. These observations were similar to those of Agelinchaab *et al.* (2006). Again, as observed by Agelinchaab *et al.* (2006), preliminary experiments also indicated that velocity profiles within porous medium rods for flows within the non-inertial range were nearly symmetric at $z = 0$. Accordingly, the velocities ranged from a maximum mid-way between adjacent rod centres, to a minimum at the rods. For these reasons, the present experiments focus on extensive velocity measurements

in the $x-y$ plane at $z/l=0$ and 0.5 locations inside the porous medium and free zone. For the case of a pair of porous media of unequal ϕ on the channel walls, the measurements were made at the two z locations using the porous medium of higher ϕ as the reference. For clarity, those locations are hereafter referred to as $z/l_{H\phi}=0$ and 0.5 for those boundary conditions. For the present experiments, the plane z/l or $z/l_{H\phi}=0$ passes between adjacent rows of the porous media rods of $\phi=0.01$, 0.025, 0.05 and 0.10. The plane z/l or $z/l_{H\phi}=0.5$ passes through the porous media rods of these models. On the other hand, due to the arrangement of porous media rods of $\phi=0.22$ and 0.49, the plane $z/l=0$ or $z/l_{H\phi}=0$ rather passes through the rods while the $z/l=0.5$ or $z/l_{H\phi}=0.5$ plane passes between adjacent rows of the rods. The plane passing between rods (PBR) and the plane passing through rods (PTR) are illustrated schematically in figure 3(b) as L_1-L_1 and L_2-L_2, respectively, in the representative top view of a porous medium model. For convenience, these planes of measurement are hereafter referred to as PBR and PTR, respectively.

It should be noted that optic-based measurements of flow fields of porous media test models are optimized not only by ensuring transparency of the test section and working fluid, but also by using a perfect refractive index matching technique. Various suggestions abound in the literature about the matching of refractive indices to ensure that high-quality data images are obtained in such measurements (e.g. Budwig 1994; Cui & Adrian 1997; Zitoun, Sastry & Guezennec 2001; Stöhr, Roth & Jähne 2003). In more recent experiments, Moroni *et al.* (2007) and Huang *et al.* (2008) have also used fluid and solid materials of identical refractive index to conduct optic-based measurements in arrangements of model porous media of varying degrees of complexity. In the former, the media was composed of homogeneous and heterogeneous matrices of beads, while in the later, the media consisted of irregularly packed spheres. As shown in figure 4, however, velocity vectors of reasonable quality were obtained even with the use of water and fluorescent particles in the PIV arrangement, by using appropriate filters in processing the data acquired. The quality of the vectors was however dependent on the solid volume fraction of the porous medium and evidence of this is given in later sections. The reduced data quality associated with solid volume fraction has therefore been accounted for in the uncertainty assessments of the measured velocities, and in the choice of results presented in this paper.

2.3. *Determination of sample size, accuracy of velocities and measurement uncertainties*

A primary concern was the sample size N necessary to achieve statistical convergence. To determine this, measurements were made for flow in the empty channel and u was evaluated using different sample sizes in the range $30 \leqslant N \leqslant 150$. The results in figure 5 indicate that within the sample range used, the velocity profiles were independent of the sample size. A minimum sample size of $N=30$ images was therefore used in subsequent measurements. In figure 5 the transverse dimension is normalized by the depth of the channel. The velocities in figure 5(a) are normalized by the streamwise bulk velocity

$$u_b = \frac{1}{H}\int_{-H/2}^{H/2} u\,\mathrm{d}y. \tag{2.2}$$

The profiles obtained were parabolic and, as expected, the ratio of the centreline velocity to u_b was 1.5 in each case.

The accuracy of the velocities obtained from the PIV was ascertained by obtaining velocity profiles of an empty channel flow at different bulk velocities and streamwise

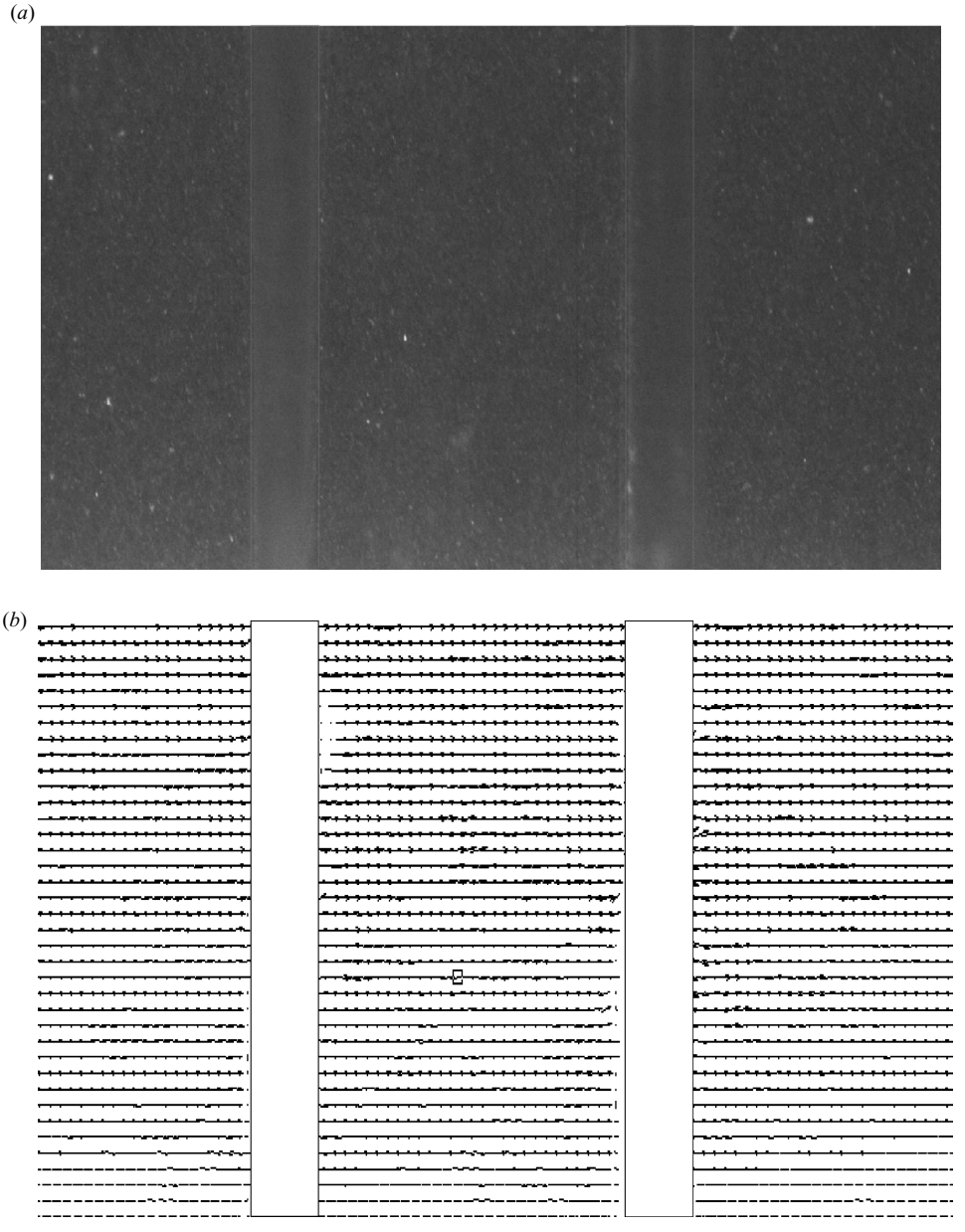

FIGURE 4. Typical (*a*) digital image; (*b*) vectors obtained from PIV measurements.

locations were compared with analytically derived results. The velocity u was normalized by the corresponding local maximum velocity u_{max}. This is demonstrated in figure 5(*b*), and it can be seen that the measured profiles are in good agreement with the analytical profile. These indicate that the flow in the empty channel is fully developed at the location of the porous media (that is, $x \geqslant 0$) as expected for a laminar flow.

To assess the measurement uncertainty, both bias and precision errors were identified and quantified in each aspect of the measurement chain. The accuracy of

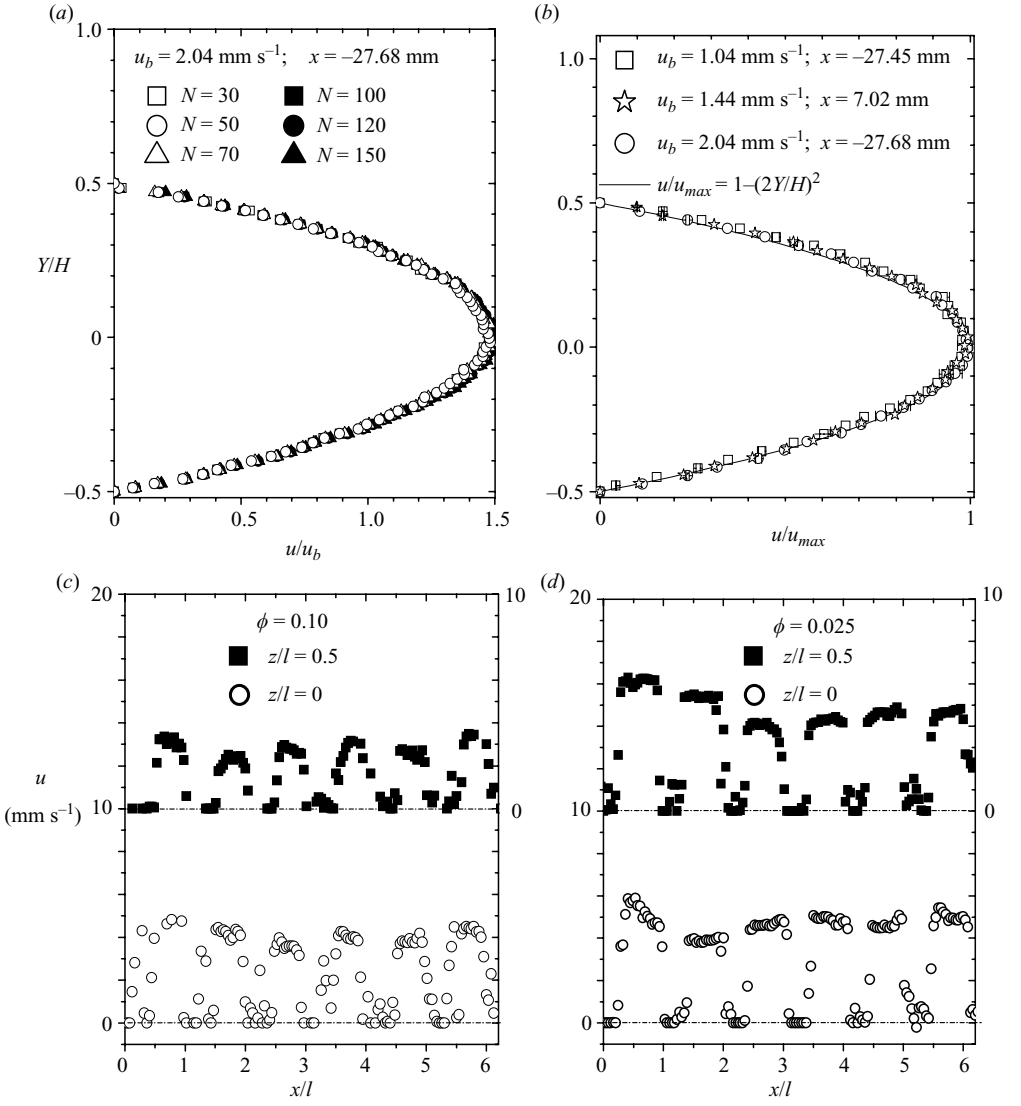

FIGURE 5. (*a*) Results of convergence test performed for an empty channel; (*b*) various profiles for flow in the mid-plane of the channel span ($z/l = 0$); (*c*) and (*d*) show the streamwise velocity profiles at $Y/H = -0.12$ to demonstrate flow development inside rods of $\phi = 0.10$ and 0.025.

the velocity measurement by PIV is limited by the accuracy of the particle response to fluid motion, light sheet positioning, light pulse timing, the size of IA and the sub-pixel interpolation of the displacement correlation peak. As pointed out in § 2.2, a number of precautionary measures were taken to reduce errors to a minimum level. The bias limit B, of the measured velocity was determined from a root-sum-square of the elementary bias limits based on sensitivity coefficients (Coleman & Steele 1995). The relative bias error $B_r = B/u$ was determined to be about 0.68 %. The precision limit P is mainly the result of scatter in the measured data due to variations in measurements and operating conditions. This was assessed statistically from $P = Ks$, where K is the confidence coefficient, having a value of 2 for a 95 % confidence level for sample

size $N > 10$ (Coleman & Steele 1995) and s is the standard deviation of the samples. Typical values of relative precision error, $P_r = P/u$ were 1.5 % inside the porous medium and 0.4 % in the free zone. The total uncertainty in u was then determined from the square root of the sum of the squared bias and precision errors. The values were found to be approximately 2 % and 1 % of u in the porous medium and in the free zone, respectively. As indicated in § 2.2, the standard deviations of the measured velocities were found to be higher, due to optical distortions, in higher solid volume fraction porous media models. In the interior of model porous media of $\phi = 0.22$ and 0.49, therefore, the uncertainty in u was about 8 % and 11 %, respectively.

2.4. *Flow development in porous medium and spatial averaging of velocity measurements*

With the installation of the model porous media in the channel, the flow in the test section became three-dimensional. It is expected that the flow through the porous media in the x direction would become periodic after a number of rows. To determine the region of periodicity, measurements were made in the $x-y$ plane at two z locations, i.e. $z/l = 0$, 0.5 (as described in figure 3*b*). The results for measurements taken for two $x-y$ planes show that the flow generally became periodic at $x/l \geqslant 2$ (that is, from the third row onwards). For clarity, this trend is shown in figure 5(*c*, *d*) extracted along the stream at the same transverse location within the porous medium in the case of $\phi = 0.10$ and 0.025, respectively. To ensure that analysis was done only in the region of periodicity, all subsequent measurements were taken at $x/l > 2$.

The continuum model of flow through porous media makes it essential to define a volume element that is sufficiently large compared with the pore volume over which an average of a property (such as porosity) is performed (Bear 1972). The present case is that of a simple homogeneous porous medium for which porosity can be defined by a square area covered by rods. Furthermore, it was noted by Agelinchaab *et al.* (2006) that for such a model, at a given transverse location of the periodic region, the velocity obtained from spatially averaging the velocities in a single square array of rods is similar to that obtained from four square arrays. Thus, for each $x-y$ plane measured, it was sufficient to average whole-field velocities at common y locations between adjacent rods (at $x/l > 2$). This was done in order to determine the representative average velocities at those y locations. This method of averaging is hereafter referred to as 'line-averaging'. Streamwise velocity (u) data sets were line-averaged using a MATLAB script. With reference to figure 3(*b*), velocities taken in the PBR were typically line-averaged from rod centre A_1 to A_2, and in the PTR, from rod centre B_1 to B_2. In either case of plane measurement, the line-averaged streamwise velocity $\langle u \rangle$ was obtained using the following relationship at a given $y = c$ location:

$$\langle u \rangle = \frac{1}{l} \int_{-l/2}^{l/2} u(x, y = c)\, \mathrm{d}x. \tag{2.3}$$

2.5. *Checks for inertial effects*

Darcy's law for a single-phase fluid flow through porous media is valid in sufficiently low-Reynolds-number regimes. The Reynolds number in this work is defined by $Re = \langle u_b \rangle d_L/\nu$. The bulk line-averaged streamwise velocity is $\langle u_b \rangle = [\int_{-H/2}^{H/2} (\langle u \rangle \mathrm{d}y)]/H$. This Re is a global Reynolds number of the flow in the test section at the location of interest. The Reynolds numbers in prior investigations (e.g. Tachie *et al.* 2004; Agelinchaab *et al.* 2006) have been at most 1. Preliminary tests conducted with the pump showed that at very low flow rates (i.e. $u_b < 1\,\mathrm{mm\ s^{-1}}$ for

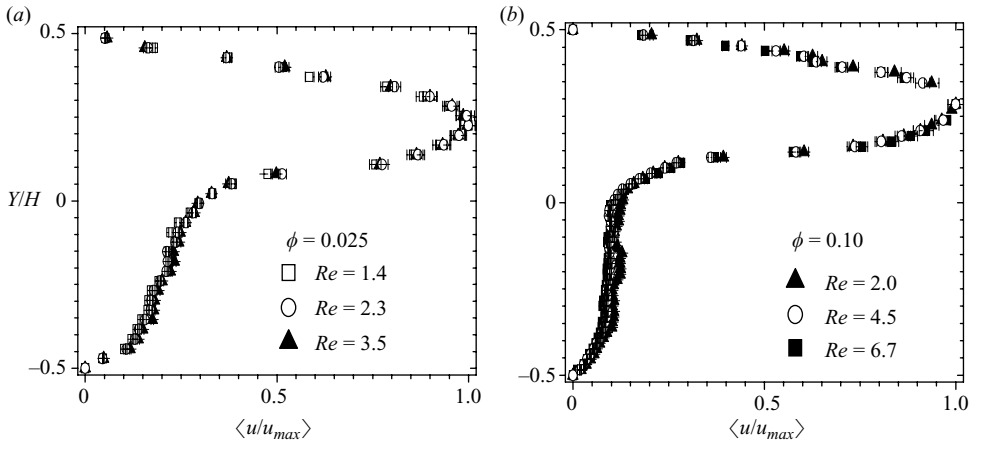

FIGURE 6. Effect of Reynolds number Re on the flow through channel with model porous medium on lower wall of $\phi =$ (a) 0.025 and (b) 0.10. Results show that within experimental errors, the flow under consideration is independent of inertial effects within the range $1.4 < Re < 6.7$.

$H = 25$ mm in a channel with no porous media present), there tended to be regions of back-flow. This resulted in sinusoidal mean velocity profiles even in the region of fully developed flow in the channel. Besides this constraint, the smallest rods in this study were of diameter $d = 1.59$ mm, and the working fluid used was water of kinematic viscosity $\nu = 1 \times 10^{-6}$ m^2 s^{-1} at 20°C. It was therefore evident that the present test conditions would yield $Re > 1$. A test of inertial effects was thus needed. To do this, velocity measurements were made for model porous media of $\phi = 0.025$ and 0.10 on the lower wall only, and at various bulk velocities. This was done to cover the range $1.4 \leqslant Re \leqslant 6.7$. In figure 6, the line-averaged streamwise velocity, $\langle u \rangle$ is normalized by the maximum line-averaged streamwise velocity $\langle u_{max} \rangle$. The data sets collapse reasonably well. Based on these results, it can be concluded that for the range of Re considered in this work, the effects of inertia are negligible.

2.6. *Test conditions*

Based on the results from the preliminary experiments, detailed measurements were made at the test conditions summarized in table 1. The experiments were conducted in three series with each set of experiments testing a specific boundary condition. In Series 1 (shown in table 1a), the model porous medium was installed on the lower wall of the channel only, with a free zone over the porous medium. These arrangements are similar to previous experimental set-ups (e.g. Agelinchaab *et al.* 2006) in which the porous medium was adjacent to a free zone. In the present case, H was kept constant at 25 mm, while ϕ was varied from 0.01 to 0.49. In Series 2 (as shown in table 1b), model porous media of equal ϕ were installed on the lower and upper walls. In Series 3 (shown in table 1c), model porous media of unequal ϕ were installed on the lower and upper walls of the channel. In Series 2 and 3, two channel depths $H \approx 22$ and 25 mm were used. In the former depth, the porous media on the lower and upper channel walls were just touching, while in the latter depth, there was a free zone between the lower and upper porous media. For each of the test conditions in Series 2, measurements were made in the planes $z/l = 0,\ 0.5$ In Series 3 experiments, where pairs of porous media of unequal ϕ were combined, measurements were made at $z/l_{H\phi} = 0,\ 0.5$ locations.

(*a*)

H (mm)	d_L (mm)	l_L (mm)	ϕ_L	$\langle u_b \rangle$ (mm s^{-1})	Re_L
25	1.59	12.60	0.01	0.71	1.1
25	1.59	8.90	0.025	0.55	0.9
25	3.18	12.60	0.05	0.66	2.1
25	3.18	8.90	0.10	0.59	1.9
25	3.18	6.03	0.22	0.56	1.8
25	4.76	6.03	0.49	0.60	2.9

(*b*)

H (mm)	d_L (mm)	d_U (mm)	l_L (mm)	l_U (mm)	ϕ_L	ϕ_U	$\langle u_b \rangle$ (mm s^{-1})	Re_L, Re_U
22	1.59	1.59	12.60	12.60	0.01	0.01	1.00	1.6
22	1.59	1.59	8.90	8.90	0.025	0.025	0.66	1.1
22	3.18	3.18	12.60	12.60	0.05	0.05	0.89	2.8
22	3.18	3.18	8.90	8.90	0.10	0.10	0.41	1.3
22	3.18	3.18	6.03	6.03	0.22	0.22	0.05	0.1
22	4.76	4.76	6.03	6.03	0.49	0.49	0.01	0.1
25	1.59	1.59	12.60	12.60	0.01	0.01	1.05	1.7
25	1.59	1.59	8.90	8.90	0.025	0.025	1.05	1.7
25	3.18	3.18	12.60	12.60	0.05	0.05	0.88	2.8
25	3.18	3.18	8.90	8.90	0.10	0.10	0.73	2.3
25	3.18	3.18	6.03	6.03	0.22	0.22	0.09	0.3
25	4.76	4.76	6.03	6.03	0.49	0.49	0.40	1.9

(*c*)

H (mm)	d_L (mm)	d_U (mm)	l_L (mm)	l_U (mm)	ϕ_L	ϕ_U	$\langle u_b \rangle$ (mm s^{-1})	Re_L	Re_U
22	3.18	1.59	12.60	12.60	0.05	0.01	0.87	2.8	1.4
22	3.18	3.18	8.90	6.03	0.05	0.22	0.74	2.3	2.4
22	3.18	4.76	12.60	6.03	0.05	0.49	0.95	3.0	4.5
22	3.18	1.59	6.03	12.60	0.22	0.01	0.68	2.2	1.1
22	3.18	3.18	6.03	12.60	0.22	0.05	0.53	1.7	1.7
25	1.59	3.18	12.60	12.60	0.01	0.05	1.05	1.7	3.3
25	3.18	1.59	12.60	12.60	0.05	0.01	1.05	3.3	1.7
25	3.18	3.18	8.90	6.03	0.05	0.22	0.10	0.3	0.3
25	3.18	4.76	12.60	6.03	0.05	0.49	0.73	2.3	3.5
25	3.18	1.59	6.03	12.60	0.22	0.01	0.88	2.8	1.4
25	3.18	3.18	6.03	12.60	0.22	0.05	0.46	1.5	1.5
28	3.18	3.18	6.03	12.60	0.22	0.05	1.16	3.7	3.7
31	3.18	3.18	6.03	12.60	0.22	0.05	1.18	3.8	3.8

TABLE 1. Summary of test conditions for (*a*) first series (*b*) second series and (*c*) third series of experiments; $h_L = 14$ mm and $h_U = 7$ mm.

In table 1 (and in figure 2*b*, *c*), the height, diameter and length of the rods used to fabricate the model porous media on the lower wall are denoted by h_L, d_L and l_L while those on the upper wall are denoted by h_U, d_U and l_U. The solid volume fractions of the model porous media on the lower and upper walls are denoted by ϕ_L and ϕ_U, respectively. Re_L and Re_U are the characteristic global Reynolds number defined as $Re_L = \langle u_b \rangle d_L/\nu$ and $Re_U = \langle u_b \rangle d_U/\nu$. The bulk line-averaged velocity $\langle u_b \rangle$ per condition was typically found to be of the same order of magnitude for the two planes of measurement. Furthermore, apart from conditions for which $\phi_L = \phi_U = 0.22$, 0.49 at $H \approx 22$, 25 mm; and $\phi_L = 0.05$, $\phi_U = 0.22$ combinations at $H \approx 25$ mm, all the other $\langle u_b \rangle$ values were found to be consistently greater in the planes z/l, $z/l_{H\phi} = 0$ than that in the planes z/l, $z/l_{H\phi} = 0.5$. Thus, only values of $\langle u_b \rangle$ and the corresponding

Re values in the planes $z/l,\ z/l_{H\phi}=0$ are shown in table 1. The Reynolds number *Re* was kept sufficiently low (i.e. $Re<6$) so that inertia was not a factor in the flow, as concluded from figure 6.

3. Results and discussion

In this section, the effects of varying boundary conditions on flow through a model porous medium are considered in order of complexity of the resulting flow. The flow through a porous medium bounded by a free zone is first discussed, followed by that with porous media on lower and upper walls, with the two media just touching. Finally, the case of flow through a pair of porous media separated by a free zone is examined. In each case, communication in flow between various layers of porous media is discussed. Pertinent issues regarding slip velocities are also examined. With regards to trends in velocities, similar observations were obtained for PBR and PTR. The trends observed in the planes $z/l_{H\phi}=0$ and 0.5 in the cases of unequal pairs of porous media on the lower and upper channel walls were also similar. To highlight these similarities, only results of selected test conditions are shown in all planes of measurement. All other results are shown for those in the PBR and plane $z/l_{H\phi}=0$. The reader may refer to Arthur (2008) for details of the plane profiles omitted.

3.1. *Velocity distributions*

The velocities reported were extracted at streamwise locations between adjacent rods shown as C and D in figure 3(*b*) for the respective planes of measurements. Only selected transverse velocities are shown. In the profiles presented subsequently, u is either normalized by the local maximum velocity u_{max} or the bulk velocity u_b. While the former shows the typical profile for the respective test conditions, the latter provides an estimate for the relative distribution of flow. The line-averaged velocities $\langle u\rangle$ are similarly normalized by the local maximum line-averaged velocities $\langle u_{max}\rangle$ and the bulk velocity $\langle u_b\rangle$. The transverse distances are normalized by the respective channel depth H. Percentage flow rate distributions per unit span of the channel in the relevant porous media and free zone for the various boundary conditions are given in table 2.

3.1.1. *Flow through a porous medium bounded by a free zone*

The effects of varying solid volume fractions of a porous medium on flow through a porous medium bounded by a free zone are shown in figures 7 and 8. Figures 7(*a*) and 8(*a*, *c*) show the velocity profiles for the flow in the PBR while figures 7(*b*) and 8(*b*, *d*), respectively, show those for the flow in the PTR. In these figures, it is noted that the streamwise velocities within the porous media for the PTR are less than the corresponding PBR. This is expected because the former is in closer contact with the rods. The difference in velocity magnitudes obtained for the two planes however diminishes with increasing ϕ.

As shown in figure 7, compared with the streamwise velocities, the measured transverse velocities are negligible in the free zone. Within the porous medium, the streamwise velocities are still generally greater than the transverse velocities. For $\phi\leqslant 0.10$, for example, the transverse velocities are no more than 10 % of the streamwise velocities. Even for the case of $\phi=0.22, 0.49$, where the velocities are much less, the transverse velocities are still only a fraction of the streamwise components. Thus, the transverse velocities are not considered in the other boundary conditions.

It is also noted in figures 7 and 8 that for cases of $\phi<0.10$, the flow within the porous medium is not uniform. These observations are similar to those for the

Boundary condition	ϕ_L	ϕ_U	H (mm)	LPM (%)	FZ (%)	UPM (%)
Porous medium on lower wall only and FZ	0.01	–	25	42	58	–
	0.025	–	25	21	79	–
	0.05	–	25	38	62	–
	0.10		25	22	78	–
	0.22	–	25	1	99	–
	0.49		25	0	100	–
TPM; unequal ϕ on both channel walls	0.01	0.01	22	63	–	37
	0.025	0.025	22	67	–	33
	0.05	0.05	22	68	–	32
	0.10	0.10	22	64	–	36
TPM; unequal ϕ on both channel walls	0.05	0.01	22	53	–	47
	0.05	0.22	22	99	–	1
	0.05	0.49	22	98	–	2
	0.22	0.01	22	5	–	95
	0.22	0.05	22	1	–	99
NTPM; equal ϕ on both channel walls	0.01	0.01	25	53	31	16
	0.025	0.025	25	56	14	30
	0.05	0.05	25	59	15	25
	0.10	0.10	25	59	15	26
	0.22	0.22	25	32	67	2
	0.49	0.49	25	21	77	2
NTPM; unequal ϕ on both channel walls	0.01	0.05	25	64	9	27
	0.05	0.01	25	63	8	29
	0.05	0.22	25	38	43	19
	0.05	0.49	25	62	7	31
	0.22	0.01	25	62	9	29
NTPM; unequal ϕ on both channel walls, varying H	0.22	0.05	25	0	36	64
	0.22	0.05	28	5	57	38
	0.22	0.05	31	2	59	39

TABLE 2. Summary results of percentage flow rate distributions for various boundary conditions of porous medium flow in PBR and plane $z/l_{H\phi} = 0$. LPM: lower porous medium; FZ: free zone; UPM: upper porous medium; TPM: touching porous media; NTPM: non-touching porous media.

area-averaged measurements of Agelinchaab *et al.* (2006). In their experimental study of a creeping flow through a model fibrous medium, Zhong, Currie & James (2006) showed that wall effects are prominent even when rods are of an aspect ratio of 31. The result of the wall effects was bulk velocities within the porous medium deviating from the Darcy velocity by as much as 15 %. However, the non-uniform nature of the velocities in this case is not just attributable to the lower wall. For such a depth of low ϕ porous medium, the boundary layers at the interface and on the lower channel wall extend to such levels within the porous medium that the result is non-uniform velocity profiles. On the other hand, the profiles in figures 7 and 8 indicate that the effects due to the interface and lower channel wall generally fade with increasing ϕ. It is therefore likely that these boundary layer effects would decrease considerably in porous media of very high ϕ such as those found in rocks and oil and gas reservoirs.

The normalized plots of figure 8(a, b) show that the phenomenon of decreasing viscous wall effects is dependent on the spacing between adjacent rods l. This explains why the velocity gradients within porous medium of $\phi = 0.025$ where $l = 8.9$ mm, are less than that of $\phi = 0.05$ where $l = 12.6$ mm. For $\phi > 0.10$, the profile becomes more

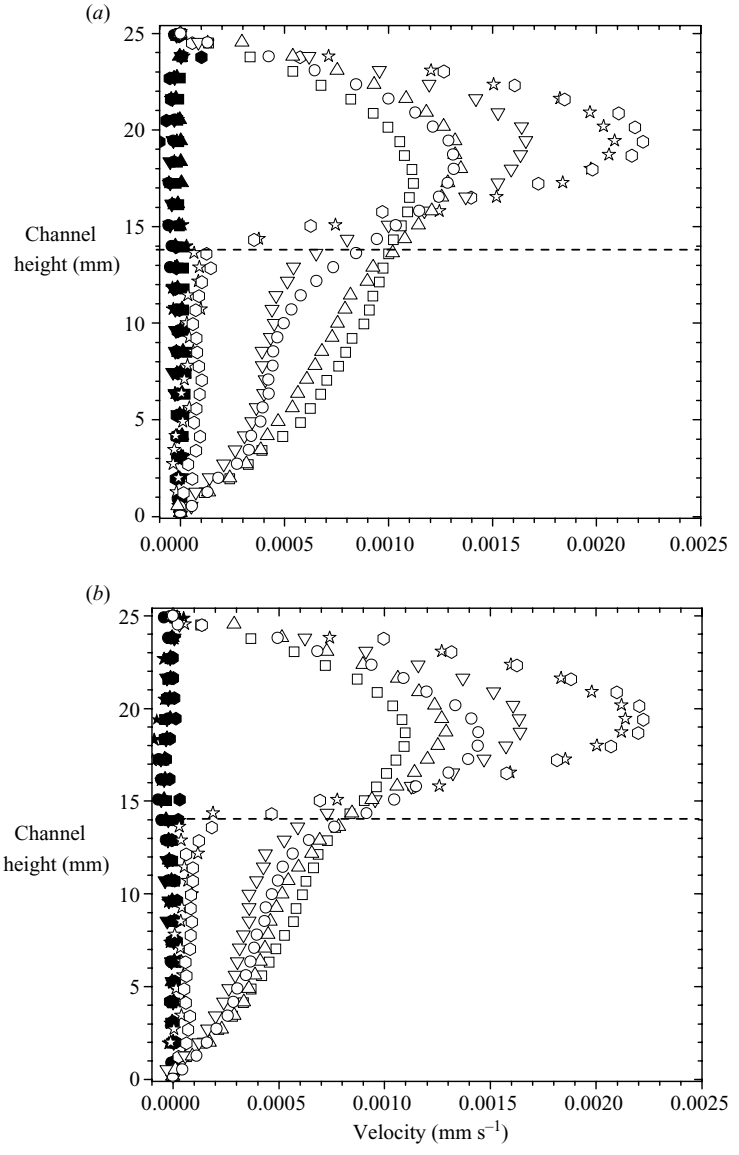

FIGURE 7. Streamwise velocity (u) and transverse velocity (v) plots for the case of flow through porous medium, bounded by a free zone. (a) Profiles for PBR and (b) for the case of PTR. The symbols used are: □ 0.01, u; ■: 0.01, v; ○: 0.025, u; ●: 0.025, v; △: 0.005, u; ▲: 0.05, v; ▽: 0.10, u; ▼: 0.10, v; ⬡: 0.22, u; ⬢: 0.22, v; ☆: 0.49, u; ★: 0.49, v. The profiles were extracted from the following locations: $\phi = 0.01$, $x/l = 4.5$; $\phi = 0.025$, $x/l = 5.5$; $\phi = 0.05$, $x/l = 5.5$; $\phi = 0.10$, $x/l = 5.5$; $\phi = 0.22$, $x/l = 3.5$; $\phi = 0.49$, $x/l = 3.5$. The dashed line is $y_1/H = 0$.

parabolic in the free zone. Unlike the empty channel for which the maximum velocity occurred on the centreline ($Y/H = 0$), the location of $\langle u_{max} \rangle$ in the present case is shifted towards the upper channel wall. This is due to the resistance in flow caused by the presence of the porous medium. The shift in the position of the $\langle u_{max} \rangle$ is minimal at $\phi = 0.01$. At $\phi = 0.49$, however, $\langle u_{max} \rangle$ is approximately mid-way the depth of the free zone.

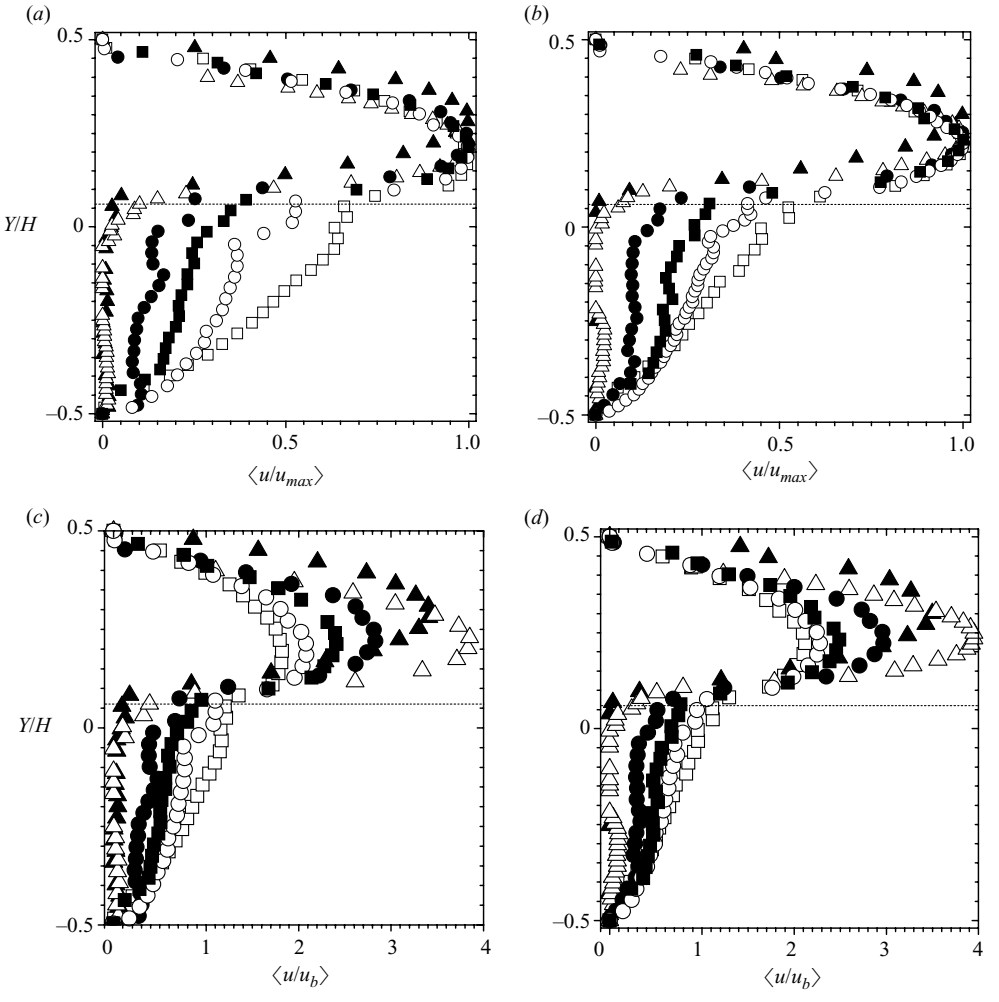

FIGURE 8. Velocity distributions for the case of model porous medium on lower wall of the channel only. $H \approx 25$ mm. The symbols used are □ $\phi = 0.01$, $l = 12.60$ mm; ■ $\phi = 0.025$, $l = 8.90$ mm; ○ $\phi = 0.05$, $l = 12.60$ mm; ● $\phi = 0.10$, $l = 8.90$ mm; △ $\phi = 0.22$, $l = 6.03$ mm; ▲ $\phi = 0.49$, $l = 6.03$ mm. (*a*, *c*) show the profiles for the flow in a PBR, and (*b*, *d*) show profiles for the flow in a PTR. The dashed line is $y_1/H = 0$.

The relative flow distributions between the various layers are shown in figure 8(*c*, *d*) and typical percentage distributions are summarized in table 2. From figure 8 (*c*, *d*), it is shown that the ratio between the maximum velocity and bulk velocity ranges from 1.5 to 4. Within this range, $\phi = 0.01$ is closest to that for an empty channel. From table 2, it is observed that the extent of flow blockage is significant even at low ϕ. For example, at $\phi = 0.01$ about 60 % of the total flow is channelled into the free zone. This value generally increases with ϕ so that $\phi = 0.22$ is just sufficient to allow no less than 99 % flow through the free zone.

3.1.2. *Flow through porous medium on lower and upper channel walls with media touching*

Figure 9 shows profiles for the case of porous media of equal ϕ on lower and upper walls. The distributions for $\phi = 0.22$, 0.49 are not shown in the figure. This is because

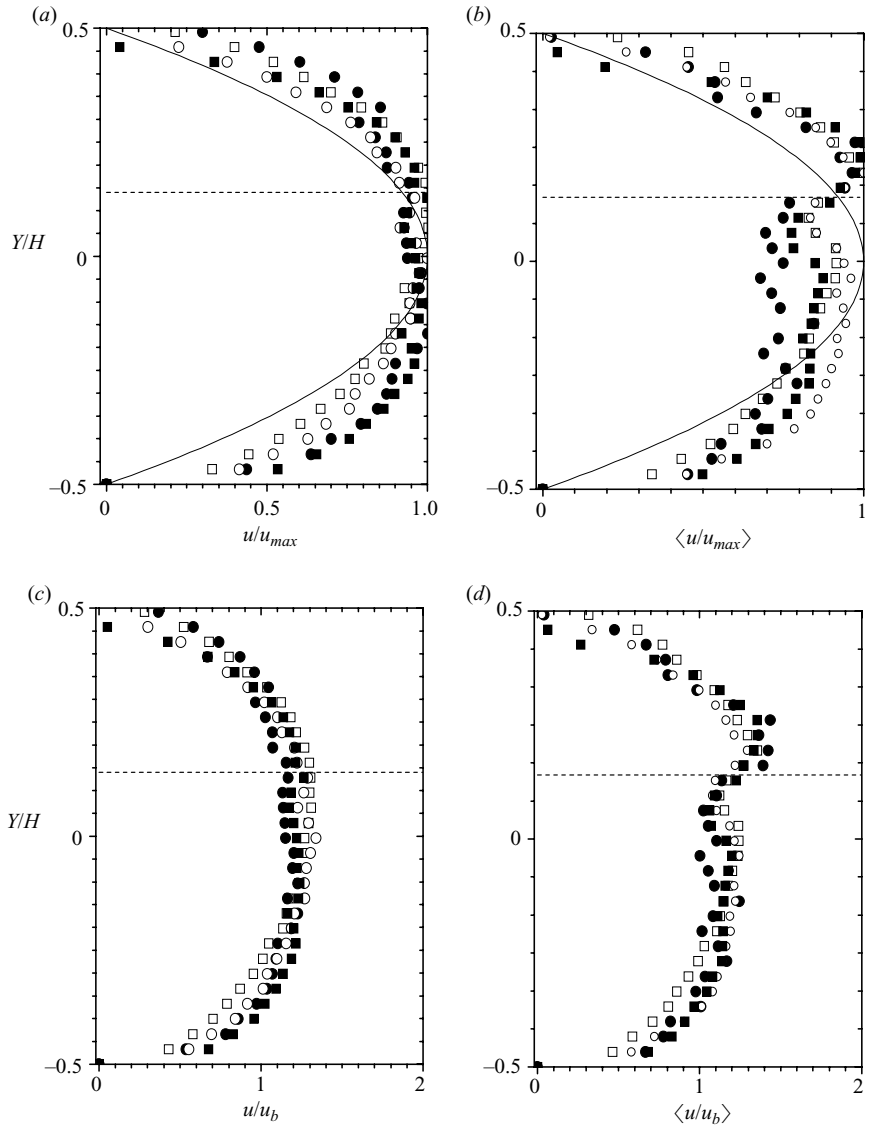

FIGURE 9. Velocity distributions for the case of model porous media of equal ϕ on both lower and upper walls of the channel in a PBR. $H \approx 22$ mm. The symbols used are □ $\phi_{LU} = 0.01$, $l = 12.60$ mm; ■ $\phi_{LU} = 0.025$, $l = 8.90$ mm; ○ $\phi_{LU} = 0.05$, $l = 12.60$ mm; ● $\phi_{LU} = 0.10$, $l = 8.90$ mm. The solid line is analytical profile for an empty channel. The profiles of figures 8(*a*, *c*) were extracted from the following locations: $\phi = 0.01$, $x/l = 4.5$; $\phi = 0.025$, $x/l = 3.5$; $\phi = 0.05$, $x/l = 4.5$, $\phi = 0.10$, $x/l = 4.5$. The dashed line is $y_1/H = 0$.

although some of these profiles show uniform velocities which are close to zero, there was significant scatter in others. The omitted datasets are shown in Arthur (2008). As indicated in figure 9(*a*), the velocity profiles for a flow through touching porous media on lower and upper channel walls follow closely those of an empty channel. However, line-averaged profiles in figure 9(*b*) show 'wake-like' patterns just above the slip plane ($y_1/H = 0$). This occurrence is due to the porous media rods on the channel

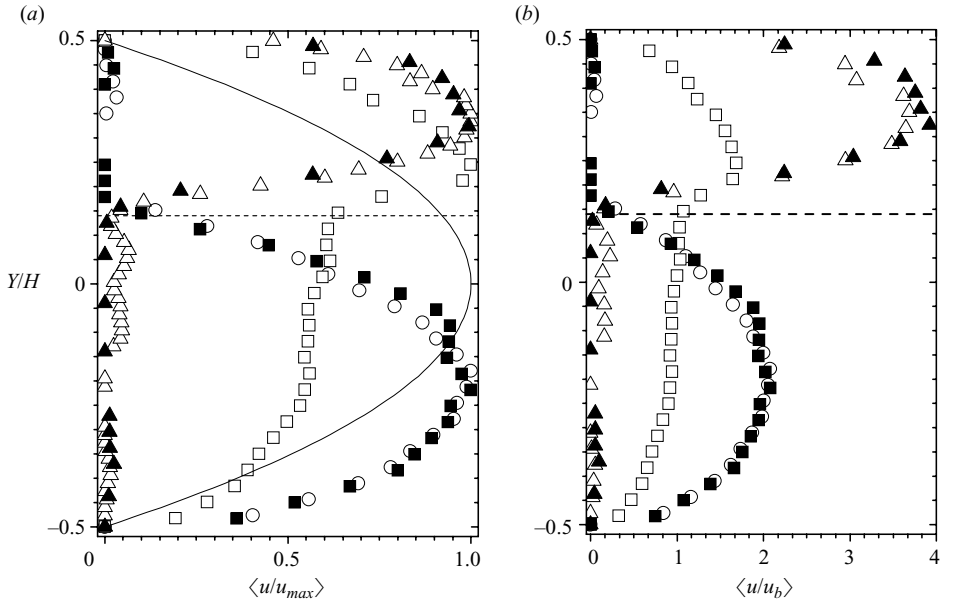

FIGURE 10. Velocity distributions for the case of model porous media unequal ϕ on both lower and upper walls of the channel. $H \approx 22$ and $z/l_{H\phi} = 0$. The symbols used are ○ $\phi_L = 0.05$, $\phi_U = 0.49$; ■ $\phi_L = 0.05$, $\phi_U = 0.22$; ▲ $\phi_L = 0.22$, $\phi_U = 0.05$; □ $\phi_L = 0.05$, $\phi_U = 0.01$; △ $\phi_L = 0.22$, $\phi_U = 0.01$. — The solid line is analytical profile for an empty channel. The dashed line is $y_1/H \approx 0$.

walls not being in perfect contact with each other. From the line-averaged velocity distributions in figures 9(*c*, *d*), and the flow rate distribution results presented in table 2, it is clear that for a pair of equal ϕ, the flow through the lower porous medium is 62 %–68 % of the overall flow. This is expected because the depth filled by the lower porous medium is about 66 % of the total channel depth. For an empty channel, the ratio u_{max}/u_b is 1.5. In this boundary condition $\langle u_{max}/u_b \rangle$ is close to this value as it varies from a minimum of 1.2 at $\phi = 0.01$ to about 1.6 at $\phi = 0.10$.

In figures 10(*a*) and 10(*b*), the $\langle u \rangle$ distributions normalized, respectively, by the local u_{max} and u_b are presented for the case where the ϕ of the lower and upper porous media are unequal. In figures 10(*a*, *b*), it is apparent that the velocity distributions are dependent on the combinations of ϕ used. As shown in figure 10(*a*), at $\phi_L = 0.01$ and 0.05, for example, there are negligible channel wall effects in ϕ_U when these porous media are combined with $\phi_U = 0.22$, 0.49. Consequently, the effect of the high ϕ_U results in a parabolic profile in the low ϕ porous medium and high shear stress regions at the interface and at the lower channel wall. When $\phi_L = 0.05$ and $\phi_U = 0.01$ pair up, the velocity profiles show relatively higher wall effects on both channel walls, as expected. The ratio of $\langle u_{max}/u_b \rangle$ is about 1.69. Although this ratio is higher than that observed for touching pairs of porous media of equal ϕ, it is close to the 1.5 value expected for the case of empty channel flow. For the cases where the ϕ values are wide apart, the ratio $\langle u_{max}/u_b \rangle$ is greater. For a high ϕ_L and a low ϕ_U (such as $\phi_L = 0.22$ and $\phi_U = 0.05$ or 0.01), $\langle u_{max}/u_b \rangle$ is about 4 while that for an arrangement of a low ϕ_L a high ϕ_U (such as $\phi_L = 0.05$ and $\phi_U = 0.22$ or 0.49) is about 2. This is because the greater the fraction of the channel depth filled by the higher ϕ, the more blockage effect results in that region, leading to more bulk flow (and a greater $\langle u_{max}/u_b \rangle$ ratio) in the region of lower ϕ.

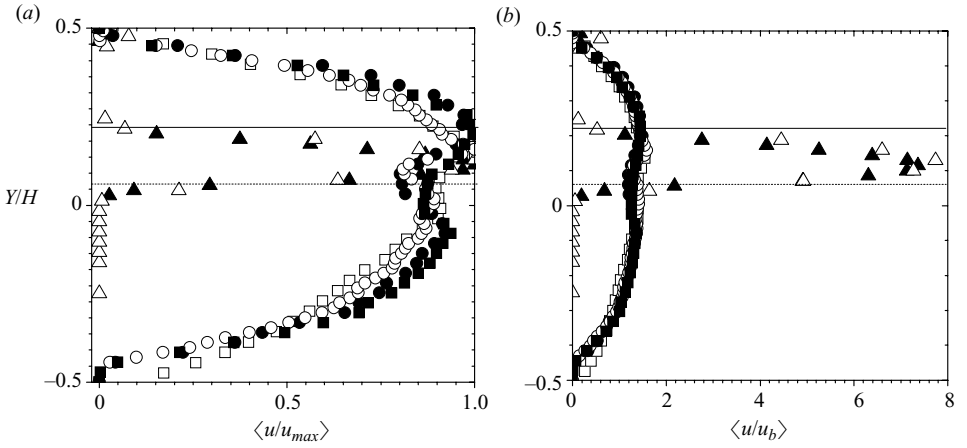

FIGURE 11. Velocity distributions for the case of model porous media of equal ϕ on both lower and upper walls in a PBR. $H \approx 25$ mm. The symbols used are □ $\phi = 0.01$, $l = 12.60$ mm; ■ $\phi = 0.025$, $l = 8.90$ mm; ○ $\phi = 0.05$, $l = 12.60$ mm; ● $\phi = 0.10$, $l = 8.90$ mm; △ $\phi = 0.22$, $l = 6.03$ mm; ▲ $\phi = 0.49$, $l = 6.03$ mm, $d = 4.76$ mm. The dashed line is $y_1/H \approx 0$, while the solid line is $y_2/H \approx 0$.

As indicated in table 2, in each of the cases of unequal ϕ pairs of touching porous media cited, it is found that there is greater flow in the porous medium with the lower ϕ if the difference in the magnitude of ϕ is high. In that case, the proportional distribution of flow is not affected by the filling fraction of the porous medium of larger ϕ. A typical case is the combination of $\phi = 0.05$ and 0.22 where at least 96 % of the bulk flow is always in the porous medium of $\phi = 0.05$ regardless of the filling fraction occupied by a medium of this ϕ. It is reasonable then to conclude that for a pair of adjoining porous media in parallel flow, there is some form of complex interchanges (flow communication) between the layers of porous media. For example, in the case where $\phi_L = 0.05$, flow through the upper porous medium increases considerably from less than 50 % of the total flow rate to about 90 % of the overall flow, as ϕ_U is varied from 0.01 to 0.22. It should be noted that, although the volume fractions of the present experiments are substantially lower than real cases, an understanding of these modes of communication provides a mental picture of what may pertain in practical applications, such as flow through coupled layers of oil or water-bearing rocks of different ϕ. In comparison with the flow bounded by the free zone, the observed flow distribution in the present boundary condition is similar. This is because in both cases, the bulk flow is skewed towards the medium of lower ϕ, where u_{max} is reached.

3.1.3. *Flow through porous media on lower and upper channel walls with media not touching*

The present section discusses the line-averaged velocity distributions for what is considered as the most complex of porous media flow investigated in this study. The profiles for porous media of equal ϕ on lower and upper walls are shown in figure 11. From figure 11(*a*) it is clear that the profiles of $\phi < 0.22$ do not show any clear boundary layer zones at $y_2/H = 0$. This is because within those ranges of ϕ, spacing between the rods of the respective porous media is significantly larger than that of the free zone separating the two porous media. The relative distribution of flow rates, as presented in table 2, shows that for $0.025 \leqslant \phi \leqslant 0.10$, the percentage

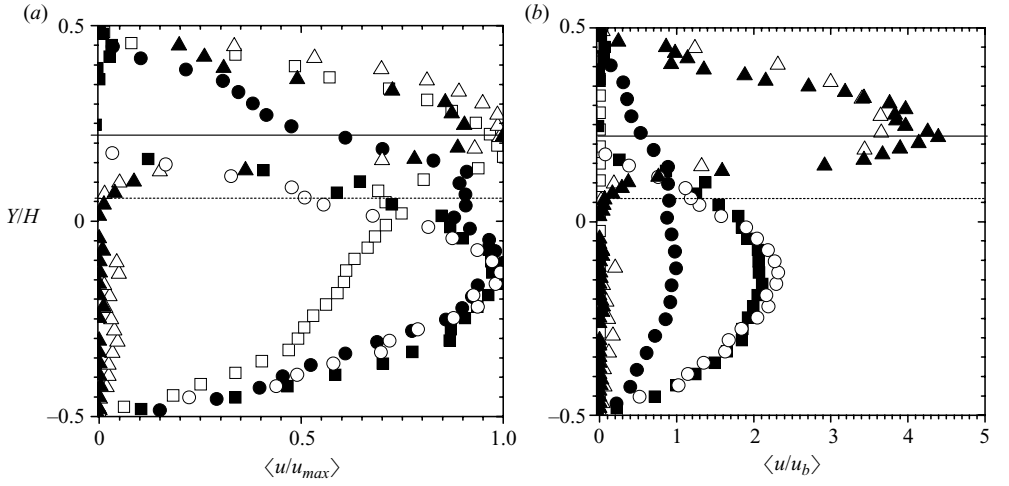

FIGURE 12. Velocity distributions for the case of model porous media unequal ϕ on lower and upper walls of the channel. $H \approx 25$ mm and $z/l_{H\phi} = 0$. The symbols used are □ $\phi_L = 0.05$, $\phi_U = 0.01$; ■ $\phi_L = 0.05$, $\phi_U = 0.22$; ○ $\phi_L = 0.05$, $\phi_U = 0.49$; ● $\phi_L = 0.01$, $\phi_U = 0.05$; △ $\phi_L = 0.22$, $\phi_U = 0.01$; ▲ $\phi_L = 0.22$, $\phi_U = 0.05$. The dashed line is $y_1/H \approx 0$ and the solid line is $y_2/H \approx 0$.

flow rates in the lower porous medium, the free zone and the upper porous medium, are nearly constant at about 57 %, 15 % and 27 %, respectively. Compared with the case of touching porous media in this ϕ range, the presence of the free zone reduces bulk flow in the upper porous medium by about 20 %, while that in the lower porous medium is reduced by about 10 %. At $\phi = 0.22$ and 0.49, parabolic flow profiles are observed in the free zone, where 67 % and 77 % of the bulk flow are respectively channelled. For these boundary conditions, as ϕ is increased from 0.22 to 0.49, the flow in the lower porous medium is reduced from 32 % to 21 % while that in the upper porous medium remains constant at 2 %. These observations are of particular importance to fluid flow through geological fractures formed when there is a separation or discontinuity plane in a geologic formation. Fractures can provide pathways for the flow of fluid, such as water or hydrocarbons, because they may possess both significant permeability and porosity. However, they are largely regarded as barriers that prevent flow across them by the reservoir engineer. The observations made for the flow through porous media with an intermediate free zone indicate a significant communication between the flow in a geological formation and an adjoining parallel fracture flow.

For unequal ϕ pairs of non-touching porous media, only line-averaged profiles are reported because the profiles are representative of the actual central location profiles. The line-averaged profiles are shown in figures 12. As observed in the case of touching porous media, when the porous media on the lower and upper walls are of unequal ϕ, the velocity distributions are determined by the combinations of ϕ used. For cases where ϕ magnitudes are wide apart (as in $\phi = 0.22$, 0.01 pair and $\phi = 0.22$, 0.05 pair), the profiles obtained are similar to those of the porous media flows bounded by a free zone, and that of touching unequal ϕ pairs of porous media. This is evident from figure 12(*a*) where in each case, a distinct boundary layer is formed at the interface between the higher ϕ and the free zone, with parabolic profiles in the free zone and lower ϕ porous medium. The communication between the porous media is more

clearly seen when the bulk distributions of figure 12(*b*) and table 2 are examined. It is observed that the distributions obtained from combinations of fairly low ϕ are not affected by the fraction filled by the porous media. For example, in combinations of $\phi = 0.01$, 0.05 the lower and upper porous media flow rates remain fairly constant at about 64 % and 28 %, respectively, regardless of the ϕ on the channel walls. However, for a combination of low and high ϕ such as in 0.05 and 0.22 combinations, there is a significant filling fraction influence. When $\phi_L = 0.05$, the flow rate per unit span in the lower porous medium is 38 % of the bulk, but when $\phi_L = 0.22$, there is no flow through the lower porous medium.

To explore the communication of flow further, the channel depth H was varied for the same rod height h for flow through a non-touching pair of porous medium. Measurements were taken for $H \approx 28$ and 31 mm. The results for the $\phi_L = 0.22$, $\phi_U = 0.05$ combination at $H \approx 28$ and 31 mm are compared with that of $H \approx 25$ mm in figure 13. From these results, it is seen that the variation of the filling fraction significantly affects the distribution of flow. At $H \approx 31$ and 28 mm, most of the bulk flow (about 58 %) is channelled through the free zone while 38 % is channelled through the upper porous medium (as shown in table 2). As the free zone is reduced to 4 mm ($H = 25$ mm), the flow distribution resembles more of an arrangement of a high ϕ porous medium on the channel lower wall only, or a combination of a low and high ϕ porous media on the upper and lower channel walls, respectively, and touching each other. In this case, 36 % and 64 % of the flow are, respectively, channelled through the free zone and the upper porous medium, as indicated in table 2. These observations imply that parallel flow communication through a porous medium and an adjoining fracture is significantly enhanced when the fracture aperture is increased, resulting in a massive influx of the bulk flow into the fracture.

3.2. *Fluid flow at the interface of a porous medium*

At the interface of a porous medium, the slip velocity U_s is perhaps the most important parameter of fluid flow. As already pointed out in the § 1, U_s is required to assess the penetration of the free zone into the porous medium. In this study, U_s is defined as the streamwise velocity at the interface between a porous medium and a free zone or another touching porous media. Only line-averaged slip velocities ($\langle u_s \rangle$) are reported. The uncertainties in using the PIV to determine this value arise from the fact that the data of particle images are averaged over a finite region to obtain a local velocity. It was therefore not always possible to locate the centre of the interrogation region on the interface itself. In the present work, it was only possible to obtain the interface within ± 0.18 mm, which corresponds to half of the side dimension of an IA. The associated relative error is estimated to be about 3 % for $\phi \leqslant 0.10$ and about 10 % for $\phi = 0.22$ and 0.49.

The slip velocities are discussed with respect to their normalizations by the respective u_{max}, and the product of the square root of the specific Darcy permeability of the porous medium and shear rate at the interface ($\dot{\gamma}\sqrt{k}$). While the former relates with the far-field maximum velocity on the flow, the latter depends on the local shear rate and permeability conditions. In order to avoid errors associated with calculating velocity gradients from experimental data, the shear rate $\dot{\gamma}$ (that is, $\mathrm{d}\langle u \rangle/\mathrm{d}y$ at the interface for the present study) was obtained as follows: a curve (of fourth-order polynomials) was fitted to the measured $\langle u \rangle$ using a least-squares method, then $\dot{\gamma}$ was obtained from a smoothed differentiation of the curve. The coefficient of determination of the curve fits was always above 0.99. The smoothing was performed over five data points, typically covering a distance of 0.15 mm, which is comparable

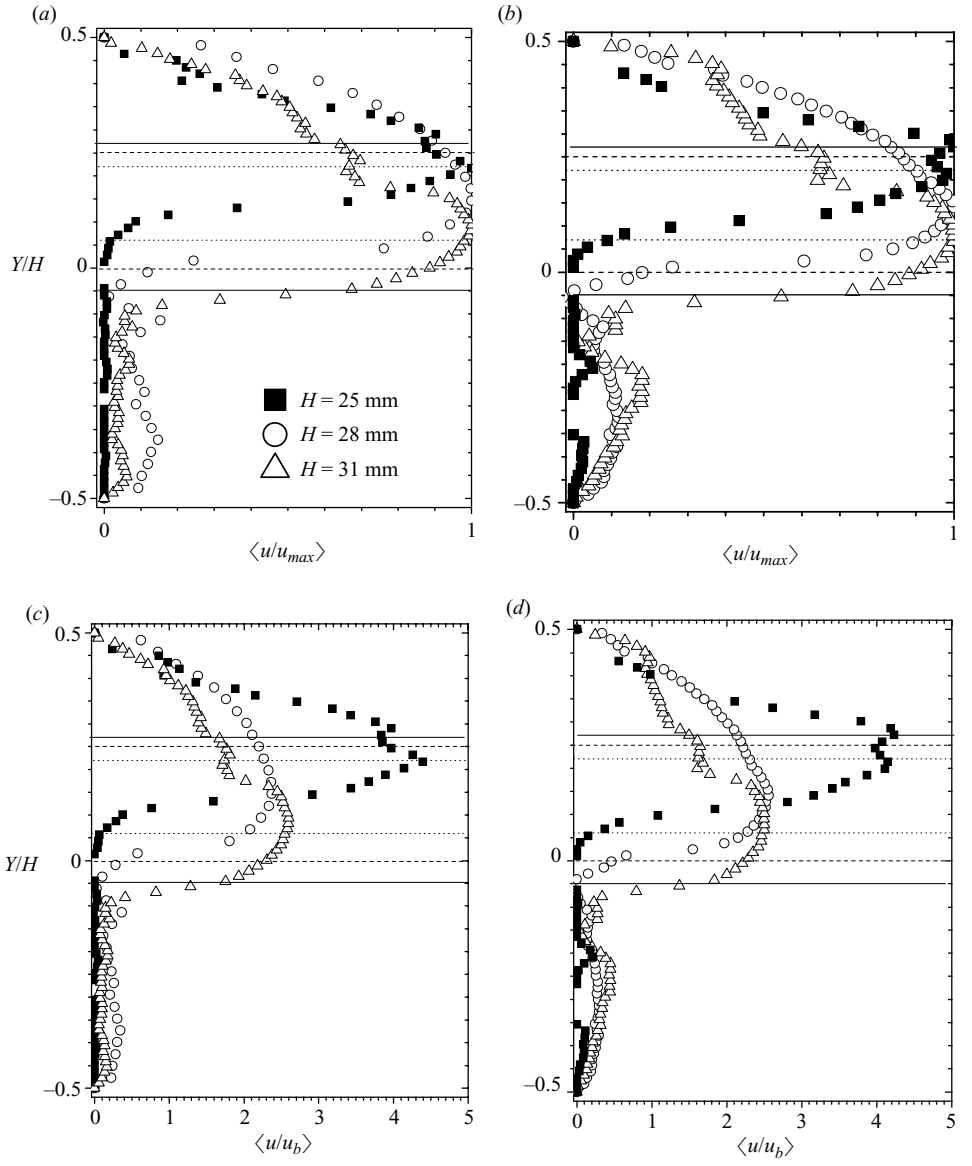

FIGURE 13. The effect of varying H for the case of porous media of $h_L = 14$ mm and $h_U = 7$ mm for $\phi_L = 0.22$, $\phi_U = 0.05$. In (a, c) measurements are in the plane $z/l_{H\phi} = 0$, and in (b, d) are in the plane $z/l_{H\phi} = 0.5$. The solid, dashed and dotted lines are lines representing approximate positions of the slip planes for $H \approx 31$, 28 and 25 mm, respectively.

with half the size of an IA. The permeability of the model porous medium, k, was obtained from (1.2). The maximum relative error due to $\langle u_s \rangle / (\dot{\gamma} \sqrt{k})$ was estimated to be 13 %.

The slip velocities for the flow through a porous medium bounded by a free zone are given in table 3. As shown, the trends in both planes are similar. Furthermore, the velocities for the present boundary condition are greater in the PBR than those in the PTR. The values of $\langle u_s \rangle$ decrease with k, showing that $\langle u_s \rangle$ depends not only on

		$\langle u_s \rangle$ (mm s^{-1})		$\dot{\gamma}$ (s^{-1})		$\langle u_s/u_{max} \rangle$		$\langle u_s \rangle/(\dot{\gamma}\sqrt{k})$	
ϕ	$\sqrt{k}$ (mm)	PBR	PTR	PBR	PTR	PBR	PTR	PBR	PTR
0.01	4.302	0.85	0.64	0.094	0.071	0.67	0.53	2.11	2.09
0.025	2.668	0.47	0.43	0.087	0.080	0.35	0.32	2.03	2.01
0.05	3.194	0.69	0.54	0.105	0.084	0.50	0.40	2.06	2.02
0.10	1.784	0.36	0.32	0.101	0.093	0.22	0.20	2.02	1.93
0.22	0.798	0.19	0.16	0.119	0.106	0.08	0.07	1.97	1.91
0.49	0.625	0.04	0.01	0.031	0.013	0.02	0.01	1.91	1.80

TABLE 3. Summary of slip velocity results for flow through porous medium on lower channel wall only.

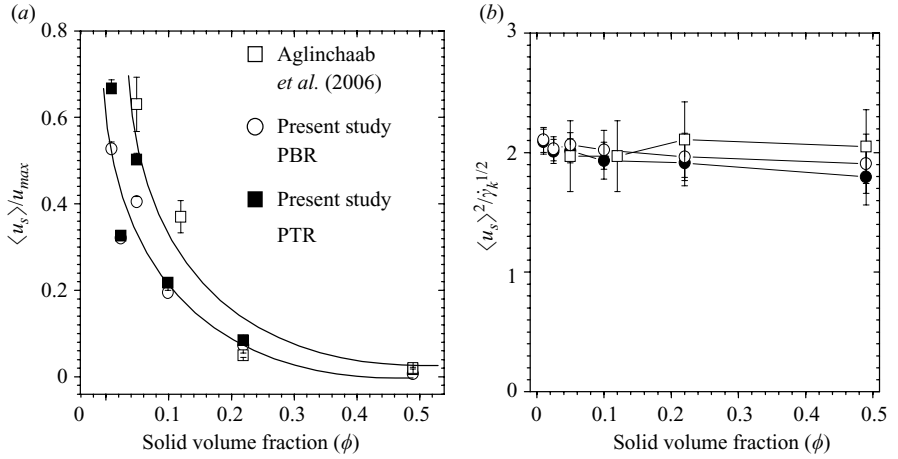

FIGURE 14. Results of present work for porous medium flow bounded by a free zone are compared with similar experimental study by Agelinchaab *et al.* (2006). The error bars represent uncertainties at 95 % confidence level in each study. Lines are used in the plots only to aid in identifying trends in the studies. As shown, the trends are in good agreement.

the solid volume fraction but also on the rod diameter and the spacing of adjacent rods of the porous medium. For a given d, $\langle u_s \rangle$ decays as l is reduced as seen in the case of $d = 1.59$ mm for porous media of $\phi = 0.01$ and 0.025 (where $l = 12.6$ and 8.9 mm respectively). Similarly, $\langle u_s \rangle$ decreases as d is increased for a given l, as observed in the cases of $\phi = 0.01$ and 0.05 where $d = 1.59$ and 3.18 mm, respectively, and $l = 12.6$ mm. This is expected because a decrease in l or an increase in d leads to a more compact porous medium arrangement, and thus a greater resistance in flow through the porous medium. As shown in table 3, $\langle u_s/u_{max} \rangle$ follow similar trends as discussed for $\langle u_s \rangle$.

The dimensionless $\langle u_s/u_{max} \rangle$ decays by about 95 % as ϕ varies from 0.01 to 0.49. For $\phi < 0.10$, $\langle u_s/u_{max} \rangle$ varies from 67 % to 20 %, showing that within this range of solid volume fraction, the slip velocity remains a significant fraction of the local maximum velocity. On the other hand, the slip velocity is no more than 8 % for $\phi \geqslant 0.22$. It is important to note that at $\phi = 0.49$ the boundary condition at the interface may be considered to be that of no-slip because $\langle u_s \rangle$ is no more than 2 % of the maximum velocity. These results concur with previous studies that for slow flow, slip velocity is only significant for $\phi < 0.10$, as in non-inertial flows over fibrous porous media

(James & Davis 2001; Davis & James 2003). Area-averaged values of Agelinchaab *et al.* (2006) for the same filling fraction and at $Re = 1$ are compared with the present results in figure 14(*a*). As shown, the trends are similar.

The dimensionless $\langle u_s \rangle / (\dot{\gamma} \sqrt{k})$ decays by just about 12 % as ϕ increases from 0.01 to 0.49. Because the decay in $\langle u_s \rangle / (\dot{\gamma} \sqrt{k})$ is just about 12 %, the values may be considered constant (that is, $\langle u_s \rangle / (\dot{\gamma} \sqrt{k}) \approx 2$) within experimental error limits. It is significant to note from table 3 that although $\langle u_s \rangle$ and $(\dot{\gamma} \sqrt{k})$ obtained from the present line-averaged measurements in PBR and PTR vary, their respective quotients (i.e. $\langle u_s \rangle / (\dot{\gamma} \sqrt{k})$) give values that are constant at 2, irrespective of the planes of measurement. Agelinchaab *et al.* (2006) also reported area-averaged values of $U_s / (\dot{\gamma} \sqrt{k}) \approx 2$ for a similar experimental set-up as presented in this work, and of the same filling fraction. As shown in figure 14(*b*), their results are in reasonable agreement with the present results within experimental error limits. In their experimental study of circular Couette flow through and over porous media of 'cross-flow' arrangement, Tachie *et al.* (2003) obtained values of $U_s / (\dot{\gamma} \sqrt{k})$ reducing from 0.30 to 0.24 as ϕ was increased from 0.01 to 0.16. In a later study, Tachie *et al.* (2004) showed that for the case of rods mounted perpendicular to the channel wall, $U_s / (\dot{\gamma} \sqrt{k})$ varied from 1.062 to 1.013 as ϕ was increased from 0.025 to 0.10. Those $U_s / (\dot{\gamma} \sqrt{k})$ values are different from the present values due to the differences in orientation of rods, and the filling fraction. As reviewed in § 1, the dimensionless slip velocity $U_s / (\dot{\gamma} \sqrt{k})$ is a very useful parameter in comparing results obtained in previous experiments because it is equivalent to the inverse of the slip coefficient α. It should be noted that the present results of $\langle u_s \rangle / (\dot{\gamma} \sqrt{k})$ are nearly twice those predicted by the Brinkman model. Beavers & Joseph (1967) obtained values equivalent to $U_s / (\dot{\gamma} \sqrt{k}) = 0.25$–10 for porous media of $\phi \approx 0.20$ (Kim & Russel 1985). This encompasses the values obtained in this work at a comparable ϕ.

For the touching and non-touching porous media, the dimensionless slip velocities were found to be more complicated, and with no systematic trend. In the former case, for example, for unequal ϕ combinations, filling fraction was a determining factor in the magnitude of $\langle u_s / u_{max} \rangle$. However, for $\langle u_s \rangle / (\dot{\gamma} \sqrt{k})$, negative values were obtained due to negative shear rate values obtained for conditions such as in $\phi_U = 0.49$ and 0.22. For the non-touching porous media $\langle u_s / u_{max} \rangle$ values were higher than those of flow through porous medium on the lower channel wall only and bounded by a free zone. The values obtained ranged over an order of magnitude as ϕ was varied within the range $0.01 \leqslant \phi \leqslant 0.49$. The dimensionless $\langle u_s \rangle / (\dot{\gamma} \sqrt{k})$ was also observed to vary considerably, not only by two orders of magnitude, but in signs and inconsistent trends that are subject to further experimental study. Due to these reasons, the slip values obtained have been omitted. It should however be noted that these complications are apparent at the interfacial regions of the velocity distributions in figures 10–12.

4. Concluding remarks

In the present work, the effects of three boundary conditions on a flow through a porous medium have been investigated experimentally. This was done using two-dimensional PIV measurements made in a pressure-driven flow through and over models of a porous medium. The models consisted of transparent acrylic circular rods arranged in a square array, ranging over $0.01 \leqslant \phi \leqslant 0.49$. The models were installed across the flow, in a rectangular channel. The models arrayed on the upper channel wall were of depth 7 mm, while those on the lower channel wall were of depth 14 mm. The Reynolds numbers were kept low so that inertia effects were negligible.

The first boundary condition studied was that of a free zone over the porous medium. At $h/H = 0.56$, the interfacial and lower wall boundary layers were found to be prominent, when $\phi \leqslant 0.10$. This resulted in non-uniform profiles within the porous medium, contrary to the predictions of the Darcy law. It was also observed that at $\phi \geqslant 0.22$, the lower wall effects were negligible and flow through the porous medium was blocked totally. It is thus sufficient to predict that velocity profiles for $\phi > 0.49$ as pertains to rocks and oil and gas reservoirs will have uniform profiles, similar to that of $\phi = 0.22$, 0.49. At the interface, $\langle u_s \rangle$ and $\langle u_s/u_{max} \rangle$ decreased with k. Furthermore, the trends of $\langle u_s/u_{max} \rangle$ and the dimensionless $\langle u_s \rangle/(\dot{\gamma}\sqrt{k})$ value of about 2 were in good agreement with area-averaged results of Agelinchaab *et al.* (2006) for a similar experimental set-up of the same filling fraction as in the present case.

For the second boundary condition, the porous medium flow was bounded by another porous medium so that the two porous media were just touching each other. The flow communication between the porous media was observed to be dependent on the relative combinations of ϕ. For a pair of equal ϕ, the flow distributions were equivalent to the fractions of the depths filled by the respective media. For unequal ϕ pairs of touching porous media, more flow was channelled to the porous medium with lower ϕ when the difference in the magnitude of ϕ was high. This phenomenon was independent of the filling fraction of the porous medium with higher ϕ. For unequal pairs of porous media, filling fraction was determinant of the magnitude of $\langle u_s/u_{max} \rangle$ while negative values of $\langle u_s \rangle/(\dot{\gamma}\sqrt{k})$ were obtained for conditions such as in $\phi_U = 0.49$ and 0.22.

In the last boundary condition, the flow through the porous medium was bounded by another porous medium with the two porous media not touching each other. For the cases of equal porous media of $\phi_L = \phi_U = 0.22$ and $\phi_L = \phi_U = 0.49$, over 60 % of the flow was channelled into the free zone between the two media. For low combinations such as $\phi = 0.01$, 0.05 the lower and upper porous media percentage distributions remained unchanged, regardless of their permutations. However, for a combination of low and high ϕ such as in 0.05 and 0.22 combinations, there was a significant filling fraction influence. Comparing $\phi_L = 0.22$, $\phi_U = 0.05$ combinations at $H \approx 28$ and 31 mm, it was observed that flow communication between layers of porous media improves with the depth of the free zone. As for the second boundary condition, the dimensionless slip velocities for the last boundary condition were also found to be complicated and lacking any systematic trend.

The present results have direct application in many systems of engineering interest such as filters and tube-in-shell heat exchangers. It also provides insights into reservoir processes such as flow in layers of soils in the ground, and in fractured reservoirs.

The financial support of this work by the Natural Sciences and Engineering Research Council of Canada through research grants to Drs D. W. Ruth and M. F. Tachie is gratefully acknowledged.

REFERENCES

Agelinchaab, M., Tachie, M. F. & Ruth, D. W. 2006 Velocity measurement of flow through a model three-dimensional porous medium. *Phys. Fluids* **18**, 017105-1–11.

Alazmi, B. & Vafai, K. 2001 Analysis of fluid flow and heat transfer interfacial conditions between a porous medium and a fluid layer. *Intl J. Heat Mass Transfer* **44**, 1735–1749.

Allan, F. M. & Hamdan, M. H. 2002 Fluid mechanics of the interface region between two porous layers. *Appl. Math. Comput.* **128**, 37–43.

Arthur, J. K. 2008 Velocity measurements of flow through a model three-dimensional porous medium with varying boundary conditions. Master of Science Thesis, University of Manitoba, Winnipeg, Manitoba.

Bear, J. 1972 *Dynamics of Fluids in Porous Media*. Elsevier.

Beavers, G. S. & Joseph, D. D. 1967 Boundary conditions at a naturally permeable wall. *J. Fluid Mech.* **30**, 197–207.

Beavers, G. S., Sparrow, E. M. & Magnuson, R. A. 1970 Experiments on coupled-parallel flows in a channel and a bounding porous medium, *J. Basic Engng Trans. A.S.M.E.* **92**D, 843–848.

Breugem, W. P., Boersma, B. J. & Uittenbogaard, R. E. 2005 The laminar boundary layer over a permeable wall. *Transp. Porous Med.* **59**, 267–300.

Brinkman, H. C. 1947 A calculation of the viscous force exerted by a flowing fluid on a dense swarm of particle. *Appl. Sci. Res.* A **1**, 27–34.

Budwig, R. 1994 Refractive index matching methods for liquid flow investigations. *Exp. Fluids* **17**, 350–355.

Chandesris, M. & Jamet, D. 2006 Boundary conditions at a planar fluid–porous interface for a Poiseuille flow. *Intl J. Heat Mass Transfer* **49,** 2137–2150.

Coleman, H. W. & Steele, W. G. 1995 Engineering application of experimental uncertainty analysis. *AIAA J.* **33**, 1888–1896.

Cui, M. M. & Adrian, R. J. 1997 Refractive index matching and marking methods for highly concentrated solid–liquid flows. *Exp. Fluids.* **22**, 261–264.

Davis, A. M. J. & James, D. F. 2003 The slip velocity at the edge of a porous medium: effects of interior resistance and interface. *Transp. Porous Med.* **53**, 175–196.

Davis, A. M. J. & James, D. F. 2004 Penetration of shear flow into an array of rods aligned with the flow. *Can. J. Chem. Engng* **82**, 1169–1174.

Deng, C. & Martinez, D. M. 2005 Viscous flow in a channel partially filled with a porous medium and with wall suction. *Chem. Engng Sci.* **60**, 329–336.

Greenkorn, R. A. 1983 *Flow Phenomena in Porous Media.* Marcel Dekker.

Gupte, S. K. & Advani, S. G. 1997 Flow near the permeable boundary of a porous medium: an experimental investigation using LDA. *Exp. Fluids* **22**, 408–422.

Huang, H. & Ayoub, J. 2008 Applicability of the Forcheimer equation for non-Darcy flow in porous media. *SPE J.* **13** (1), 112–122.

Huang, A. Y. L., Huang, M. Y. F., Capart, H. & Chen, R.-H. 2008 Optical measurements of pore geometry and fluid velocity in a bed of irregularly packed spheres. *Exp. Fluids* **45**, 309–321.

Jackson, G. W. & James, D. F. 1986 The permeability of fibrous porous media. *Can. J. Chem. Engng* **64**, 364–374.

James, D. F. & Davis, A. M. J. 2001 Flow at the interface of a model fibrous medium. *J. Fluid Mech.* **426**, 47–72.

Khalili, A., Basu, A. J., Pietrzyk, U. & Raffel, M. 1999 An experimental study of recirculating flow through fluid-sediment interfaces. *J. Fluid Mech.* **383**, 229–247.

Kim, S. & Kussel, W. B. 1985 Modelling of porous media renormalization of the Stokes equations. *J. Fluid Mech.* **154**, 269–286.

Larson, R. E. & Higdon, J. J. L. 1986 Microscopic flow near the surface of two dimensional porous media. Part 1. Axial flow. *J. Fluid Mech.* **166**, 449–472.

Larson, R. E. & Higdon, J. J. L. 1987 Microscopic flow near the surface of two-dimensional porous media. Part 2. Transverse flow. *J. Fluid Mech.* **178**, 119–136.

Moroni, M. & Cushman, J. H. 2001 Statistical mechanics with three-dimensional particle tracking velocimetry experiments in the study of anomalous dispersion. II. Experiments. *Phys. Fluids* **13**, 81–91.

Moroni, M., Kleinfelter, N. & Cushman, J. H. 2007 Analysis of dispersion in porous media via matched-index particle tracking velocimetry experiments. *Adv. Water Res.* **30**, 1–15.

Nield, D. A. & Bejan, A. 1992 *Convection in Porous Media.* Springer.

Northrup, M. A., Kulp, T. J., Angel, S. M. & Pinder, G. F. 1993 Direct measurement of interstitial velocity field variations in a porous medium using fluorescent-particle image velocimetry. *Chem. Engng Sci.* **48**, 13–21.

Ochoa-Tapia, J. A. & Whitaker, S. 1995 Momentum transfer at the boundary between a porous medium and a homogenous fluid. 1. Theoretical development. *Intl J. Heat Mass Transfer* **38**, 2635–2646.

Ochoa-Tapia, J. A. & Whitaker, S. 1998 Momentum jump condition at the boundary between a porous medium and a homogenous fluid: inertial effects. *J. Porous Media* **1**, 201–217.

Ogawa, K., Matsuka, T., Hirai, S. & Okazaki, K. 2001 Three-dimensional velocity measurement of complex interstitial flows through water-saturated porous media by the tagging method in the MRI technique. *Meas. Sci. Technol.* **12**, 172–180.

Peurrung, L. M., Rashidi, M. & Kulp, T. J. 1993 Measurement of porous medium velocity fields and their volumetric averaging characteristics using particle tracking velocimetry. *Chem. Engng. Sci.* **50** (14), 2243–2253.

Prasad A. K. 2000 Particle image velocimetry. *Curr. Sci.* **79** (1), 51–60.

Raffel, M., Willert, C., Wereley, S. & Kompenhans, J. 2007 *Particle Image Velocimetry. A Practical Guide*. Springer.

Rashidi, M., Peurrung, L., Tompson, A. F. B. & Kulp, T. J. 1996 Experimental analysis of pore-scale flow and transport in porous media. *Adv. Water Resour.* **19**, 163–180.

Richardson, S. 1971 A model for the boundary condition of a porous material. Part 2. *J. Fluid Mech.* **49**, 327–336.

Rosenzweig, R. & Shavit, U. 2007 The laminar flow field at the interface of a Sierpinski carpet configuration. *Water Resour. Res.* **43**, W10402. doi:10.1029/2006WR005801.

Saffman, P. G. 1971 On the boundary condition at the surface of a porous medium. *Stud. Appl. Math.* **50**, 93–101.

Sahraoui, M. & Kaviany, M. 1992 Slip and no-slip velocity boundary at interface of porous, plain media. *Int. J. Heat Mass Transfer* **35** (4), 927–943.

Saleh, S., Thovert, J. F. & Adler, P. M. 1992 Measurement of two-dimensional velocity fields in porous media by particle image displacement velocimetry. *Exps. Fluids* **12**, 210–212.

Sangani, A. S. & Acrivos, A. 1982 Slow flow past periodic arrays of cylinders with application to heat transfer. *Int. J. Multiphase Flow* **8**, 193–206.

Scheidegger, A. E. 1974 *The Physics of Flow Through Porous Media*. University of Toronto Press.

Shams, M., James, D. F. & Currie, I. G. 2003 The velocity field near the edge a model porous medium. *Exp. Fluids* **35**, 193–198.

Stephenson, J. L. & Stewart, W. E. 1986 Optical measurements of porosity and fluid motion in packed beds. *Chem. Engng Sci.* **41**, 2161–2170.

Stöhr, M., Roth, K. & Jähne, B. 2003 Measurement of 3D pore-scale flow in index-matched porous media. *Exp. Fluids* **35**, 159–166.

Tachie, M. F., James, D. F. & Currie, I. G. 2003 Velocity measurements of the shear flow penetrating a porous medium. *J. Fluid Mech.* **493**, 319–343.

Tachie, M. F., James, D. F. & Currie, I. G. 2004 Slow flow through a brush. *Phys. Fluids* **16** (2), 445–451.

Taylor, G. I. 1971 A model for the boundary condition of a porous material. Part 1. *J. Fluid Mech.* **49**, 319–326.

Vafai, K. & Thyagaraja, R. 1987 Analysis of flow and heat transfer at the interface region of a porous medium. *Intl J. Heat Mass Transfer* **30**, 1391–1405.

Yarlagadda, A. P. & Yoganathan, A. P. 1989 Experimental studies of model porous media fluid dynamics. *Exp. Fluids* **8**, 59–71.

Zhong, W. H., Currie, I. G. & James, D. F. 2006 Creeping flow through a model fibrous porous medium. *Exp. Fluids* **40**, 119–126.

Zitoun, K. B., Sastry, S. K. & Guezennec, Y. 2001 Investigation of three-dimensional interstitial velocity, solids motion, and orientation in solid-liquid flow using particle tracking velocimetry. *Int J. Multiphase Flow* **27,** 1397–1414.